

Linköping University Postprint

Performance evaluation of dimensionality reduction techniques for multispectral images

Pedro Latorre Carmona, Reiner Lenz

This is a postprint of an article published in:

Pedro Latorre Carmona & Reiner Lenz, Performance evaluation of dimensionality reduction techniques for multispectral images, 2007, International Journal of Imaging Systems and Technology, (17), 3, 202-217.

<http://dx.doi.org/10.1002/ima.20107> .

Copyright: John Wiley & Sons Inc., <http://www3.interscience.wiley.com/journal/37666/home>

Postprint available free at:

Linköping University E-Press: <http://urn.kb.se/resolve?urn=urn:nbn:se:liu:diva-10423>

Performance evaluation of dimensionality reduction techniques for multispectral images

Pedro Latorre Carmona¹, Reiner Lenz²

¹Depto. Lenguajes y Sistemas Informáticos, Universidad Jaume I
Campus del Riu Sec s/n, 12071, Castellón de la Plana, Spain

latorre@lsi.uji.es

²Department of Science and Technology, Linköping University, Campus Norrköping
Norrköping, Sweden

reile@itn.liu.se

We consider several collections of multispectral color signals and describe how linear and non-linear methods can be used to investigate their internal structure. We use databases consisting of blackbody radiators, approximated and measured daylight spectra, multispectral images of indoor and outdoor scenes under different illumination conditions and numerically computed color signals. We apply *Principal Components Analysis*, group-theoretical methods and three manifold learning methods: *Laplacian Eigenmaps*, *ISOMAP* and *Conformal Component Analysis*. Identification of low-dimensional structures in these databases is important for analysis, model building and compression and we compare the results obtained by applying the algorithms to the different databases.

1. Introduction

Traditional colour acquisition, visualization and printing systems describe colour information in three dimensional coordinate systems. Well-known examples are *RGB*, *CIEXYZ*, *CIELAB* and *CMY*. An exception is the *CMYK* and related printing systems [23]. This is usually sufficient for applications where a human user is involved since the human colour vision system is tri-chromatic.

One of the most important drawbacks of three-dimensional colour systems is the loss of information when coding colour in just three numbers. Many problems are related to *Metamerism*, where two materials may have the same colour coordinates but different spectral signature. They have different color properties but their differences are lost in the three-dimensional description.

Conventional colour descriptors are also restricted to electromagnetic radiation in the wavelength range most relevant for human observers, i.e. approximately 400nm to 700nm. In some applications channels in different parts of the electromagnetic spectrum or more channels are needed. Examples are industrial inspection, remote sensing, archiving of pieces of art to mention only a few.

This is the reason why new measurement devices are developed that can provide better characterizations of the colour properties. These devices are using more than three bands and some of them are also measuring contributions from the ultraviolet or infrared part of the spectrum. The result is often a large number of data vectors of relatively high dimensionality. In remote sensing applications it is, for example, common to measure hundreds of channels per pixel. These new data volumes require new methods to efficiently store and retrieve data and also new ways of understanding their properties. There is now an extensive literature on standard compression methods and their application to multispectral color signal processing but applications of new manifold learning methods are rarer and therefore we describe here our experiments in running different algorithms on the same data sets. We mention only a few articles on dimensionality reduction for multispectral color processing and the interested reader can certainly find many more: [10,18,21,27,19,2,5-7,11,26]

In this paper we investigate the use of a standard linear dimensionality reduction technique (*Principal Components Analysis*, *PCA*), and some non-linear dimensional reduction

techniques, like group theoretical methods ([14]), *Laplacian Eigenmaps (LE,[1])*, *Isometric Feature Mapping (Isomap,[25])*, and *Conformal Component Analysis (CCA,[22])*. The goal of this investigation was to find out if it is possible to find geometrical structures in spaces of color spectra. Here we understand geometrical structures in a very wide sense. The problem is thus more related to general data-mining techniques than conventional data compression. This very broad problem definition implies that it is difficult to measure the performance of the different methods. Conventional criteria like mean-squared error are not suitable since they assume that the spaces are equipped with the Euclidean norm, an assumption that is probably not valid in many cases. In many situations a simple visual inspection of the results by the user may be the only available evaluation method. In the cases where we find characteristic geometrical structures we may use them for solving application problems of great practical importance. As an example we mention color constancy: Assume we find that the time-changing illumination spectra are all located on a curve. In that case we can describe the effect of the illumination change on the measured images by a differential equation. We can then use this to compensate the effects of the illumination change or generate the appearance of the scene under a different illumination (a detailed description of such an application is described in [17]).

We apply these techniques to investigate different types of spectral data: analytically defined spectra (Plank spectra), *D-type* illuminations obtained by empirically derived approximations [9,28], a series of measurements of daylight spectra from Norrköping, Sweden and a series of multispectral images of indoor and outdoor scenes, some obtained with our own acquisition system and others from other research groups [4].

In the following section, we describe in detail the spectra used in the experiments. We also give a brief overview over the methods used. A more detailed description can be found in the appendix but for a complete description the reader is referred to the original articles. The experiments and their results are described and discussed in Experimental Results and Discussion section and conclusions can be found in Conclusions section.

2. Spectral Data and Overview over Applied Methods

We investigate the following classes of spectral data: natural illumination spectra, our own indoor images of a static scene under different illumination conditions, and the reflectance images of indoor and outdoor scenes described in [4]. The investigation of different types of illuminations is not only an interesting research issue, but we also combine those different illuminations to create *simulated* images from the reflectance images. These simulated images are used to investigate different properties of the interaction between the illumination and the object properties.

2.1. Plank spectra

Plank's Law of electromagnetic radiation describes the amount of energy irradiated by any solid or liquid body as a function of its internal temperature. This formula is often used to characterize the spectral properties of sources of radiation (see [28] for more information). If a body has an internal temperature of K degrees Kelvin, then the radiated power density follows the equation (c is the speed of light and h Planck's constant):

$$S(\lambda) = \frac{8\pi c h}{\lambda^5} \frac{1}{e^{\frac{hc}{\lambda K T}} - 1}, \quad (1)$$

In Figure 1 we show a group of 100 spectra from 3000K to 12000K. Here we sample the temperature range from 3000K to 12000K in equal steps of 1/K units, the so called *mired*

scale. This sampling is often useful in studies of human color vision since our perception of color changes is more closely related to differences in the mired scale than in the original temperature scale.

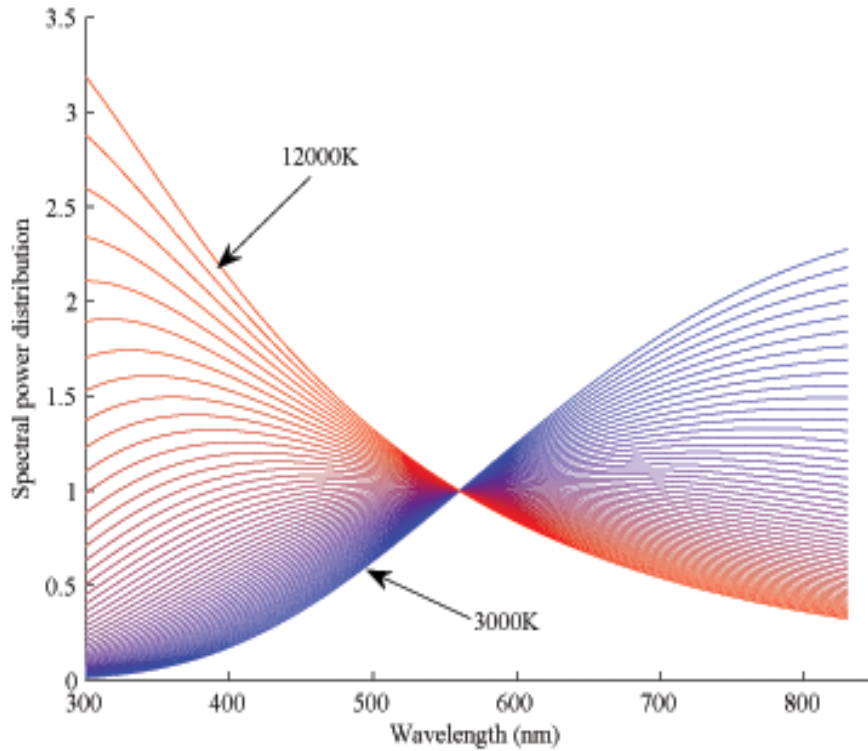


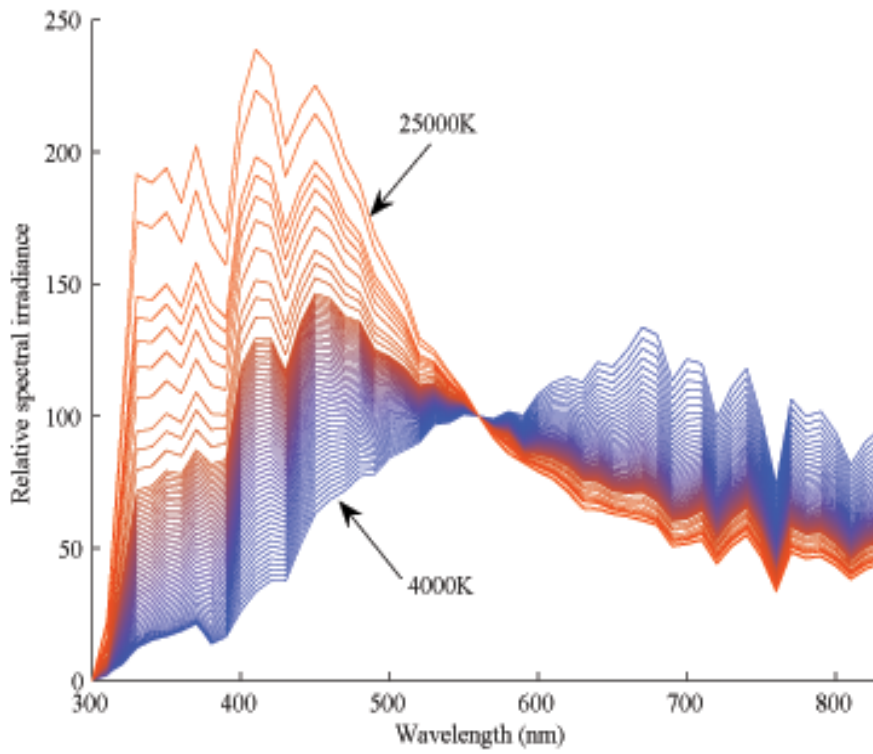
Fig. 1. Power distribution of Black Body radiators from 3000 K to 12000 K in the mired sampling

2.2. Empirical Daylight-type Illuminations

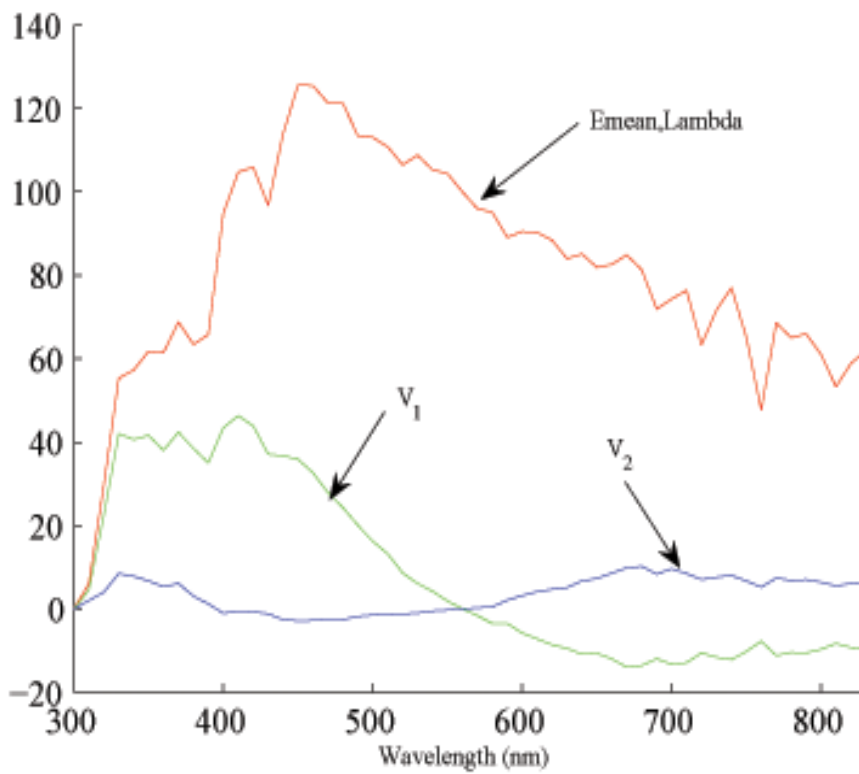
Judd et. al. showed in [9] that daylight spectra can be approximated by the linear combination of three vectors $(\overline{\mathbf{e}}_\lambda, \mathbf{v}_{1,\lambda}, \mathbf{v}_{2,\lambda})$ as:

$$\overline{\mathbf{e}}_\lambda = \overline{\mathbf{e}}_\lambda + M_1 \cdot \mathbf{v}_{1,\lambda} + M_2 \cdot \mathbf{v}_{2,\lambda}, \quad (2)$$

where M_1 and M_2 are weights and $(\overline{\mathbf{e}}_\lambda, \mathbf{v}_{1,\lambda}, \mathbf{v}_{2,\lambda})$ are empirically obtained to optimally recover a database of measured daylight spectra. We call the spectra obtained by this formula *D-type* spectra. In Figure 2(a) we show a group of *D-type* spectra from 4000 K to 25000 K and in (b) we show the shape of the three vectors used in [9].



(a)



(b)

Fig. 2. (a) Simulated spectral irradiance of daylight from 4000K to 25000K based on Eq. 2, (b) Vectors used in Eq. 2

2.3. Database of natural spectra measured in Norrköping, Sweden

This Database was measured by the Swedish Meteorological and Hydrological Institute (SMHI). It consists of 21871 daylight spectra measured between June 16, 1992 and July 7, 1993. Measurements were made every 5 minutes, and the wavelength range was 380nm to 780nm in 5nm steps.

2.4. Multispectral images of a static scene with variable illumination

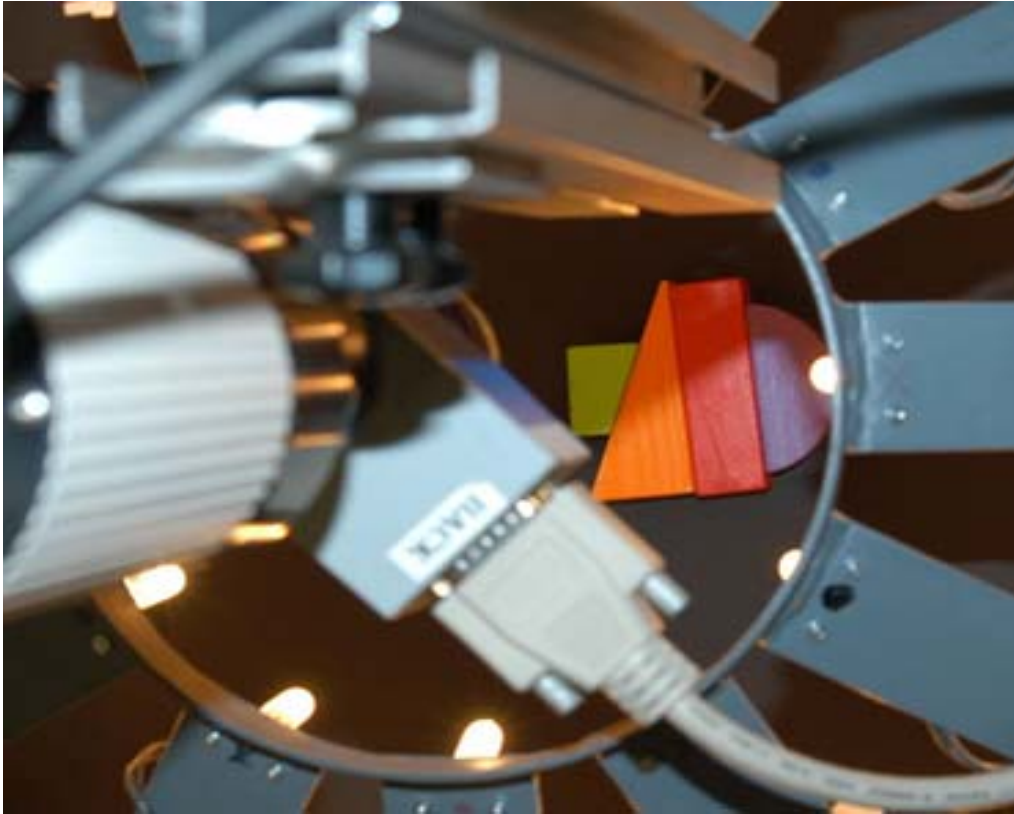
We use a multichannel camera based on the CCD *QImaging* Retiga EX camera (12-bit, Monochrome Cooled camera without IR Filter). The sensor resolution is 516×676 pixels. Attached to the camera is a *Liquid Crystal Tuneable Filter* (LCTF), which provides a spectral sampling of 10 nm in the range from 400 to 720 nm, resulting in 33 channels. The filter is fixed in front of the camera.

We use a hemisphere-like illumination structure with a diameter of 60 cm. It has 120 halogen lights of 10 Watts each. The lamps are powered by three-phase AC 12 volts adjustable power supply. Each group powers 40 lamps. Therefore, effects like flickering are avoided. The voltage level of the illumination chamber can be changed leading to changes in the spectral power distribution of the illuminant. The experimental set-up is shown in Figure 3(a).

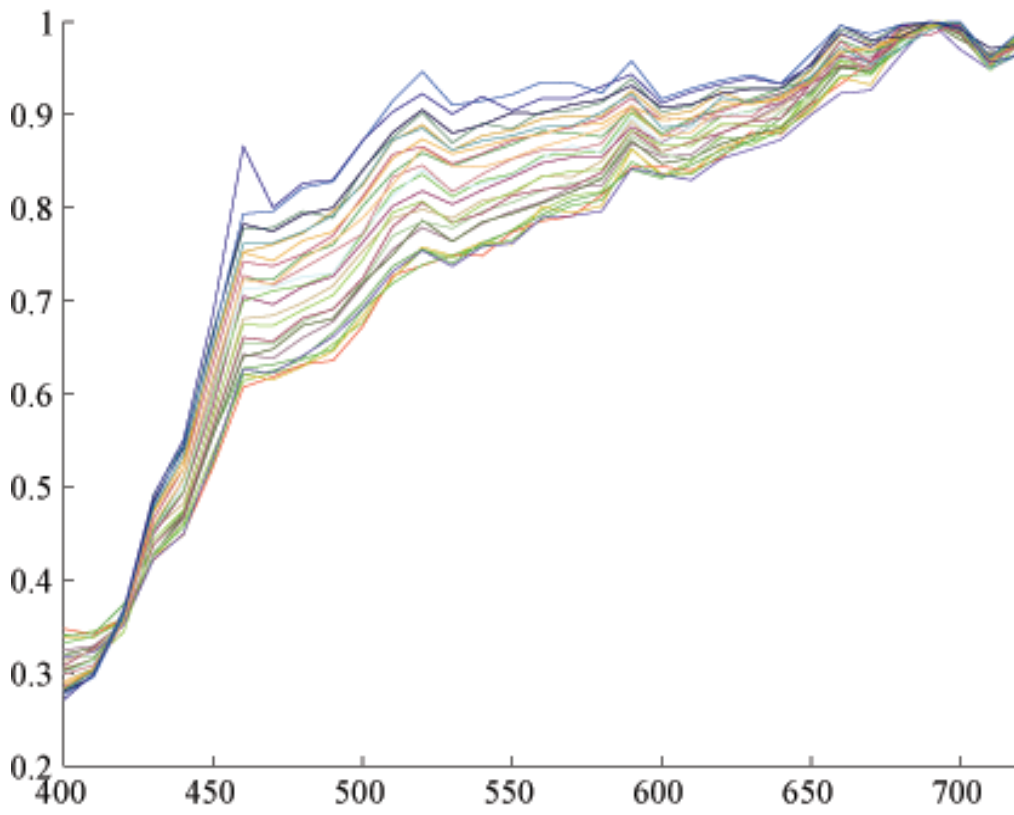
We change the power supply of the illumination uniformly over the whole range to get 26 different illuminations and for each illuminant we capture an image of a perfect reflectance diffuser object (*spectralon*) to serve as a spectral descriptor of the light source. In Figure 3(b) a close-up of the figures imaged with the multispectral camera is shown. In Figure 3(c) the spectral power distributions of the illuminants are plotted. They are normalized to 1 dividing each one by its own maximum.



(a)



(b)



(c)

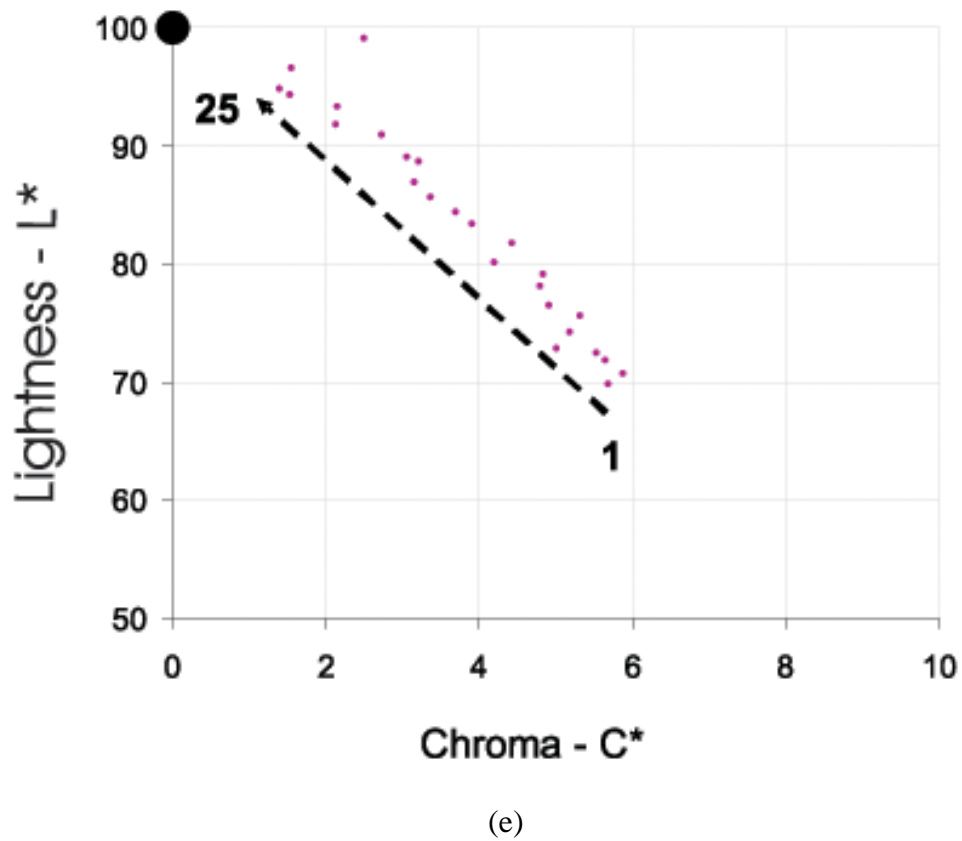
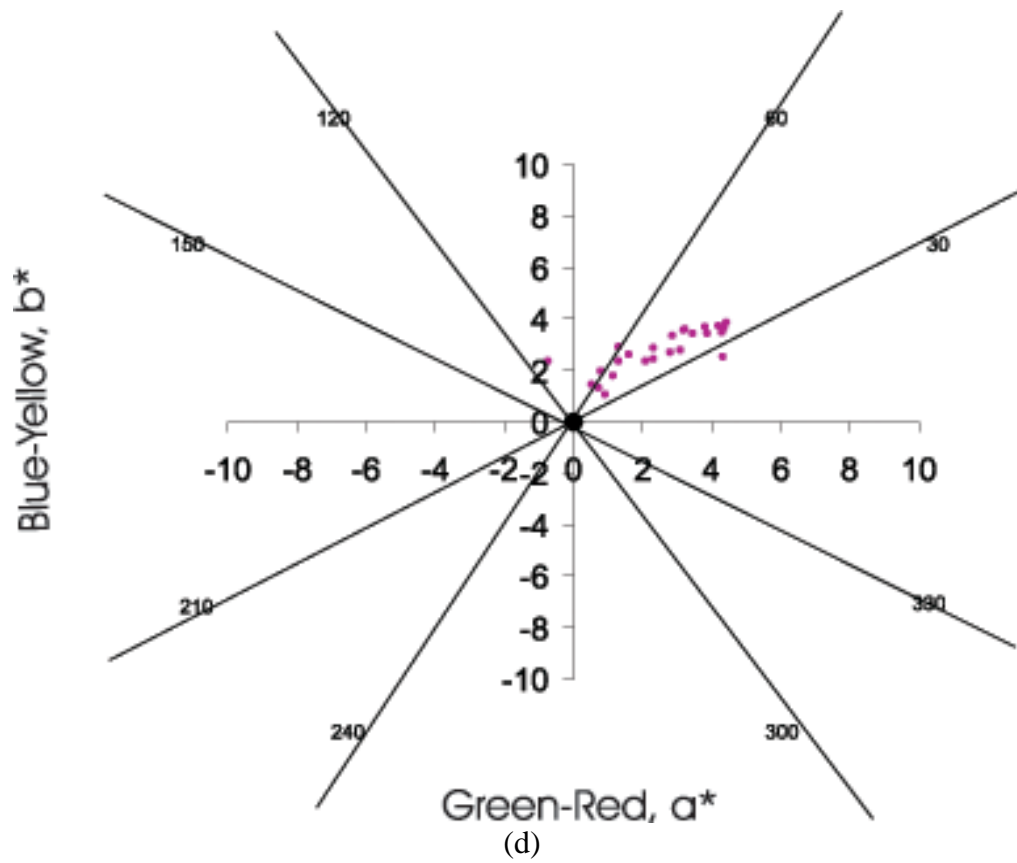


Fig. 3. (a) Experimental set-up, (b) close-up showing the coloured wooden figures, (c) Normalized spectra of the 26 illumination levels, (d) a^* vs b^* chromaticity representation, (d) Lightness vs. Chroma.

To assess the colour difference among the different illumination spectra, we use the *CIELAB* colour space. First we compute the CIEXYZ coordinates of the *spectralon* (see [8]):

$$X \propto \sum_{\lambda} P(\lambda)R(\lambda)\bar{x}(\lambda), \quad Y \propto \sum_{\lambda} P(\lambda)R(\lambda)\bar{y}(\lambda), \quad Z \propto \sum_{\lambda} P(\lambda)R(\lambda)\bar{z}(\lambda) \quad (3)$$

where $P(\lambda)$ is the power distribution of the illuminant, $R(\lambda)$ is the reflectance spectrum of the *spectralon* and the product $P(\lambda) \cdot R(\lambda)$ is the signal arriving at the camera. $[\bar{x}(\lambda), \bar{y}(\lambda), \bar{z}(\lambda)]$ are the *Colour Matching Functions* of the 10° 1964 *CIE Supplementary Standard Observer* [8]. The *white point* for the different illuminations (X_{ni}, Y_{ni}, Z_{ni}) , $i = 1, \dots, 26$, is obtained evaluating the XYZ coordinates of the those images, and normalizing the Y value of the highest illuminant to 100. The rest of the (X_{ni}, Y_{ni}, Z_{ni}) values are changed accordingly:

$$X_{ni} \leftarrow \frac{X_{ni}}{Y_{n26}} \cdot 100, \quad Y_{ni} \leftarrow \frac{Y_{ni}}{Y_{n26}} \cdot 100, \quad Z_{ni} \leftarrow \frac{Z_{ni}}{Y_{n26}} \cdot 100. \quad (4)$$

This normalization constant is used for any *CIELAB* computation. In Figure 3 (d) and (e) we show how the *Luminance* as well as the *Chromaticity* changes for the different illuminations. Once the change in illumination has been assessed, we acquire a series of 26 images of 4 wooden geometric objects (denoted as Image1 to Image26) for the same changes in illumination.

2.5. Multispectral Images of Natural Scenes

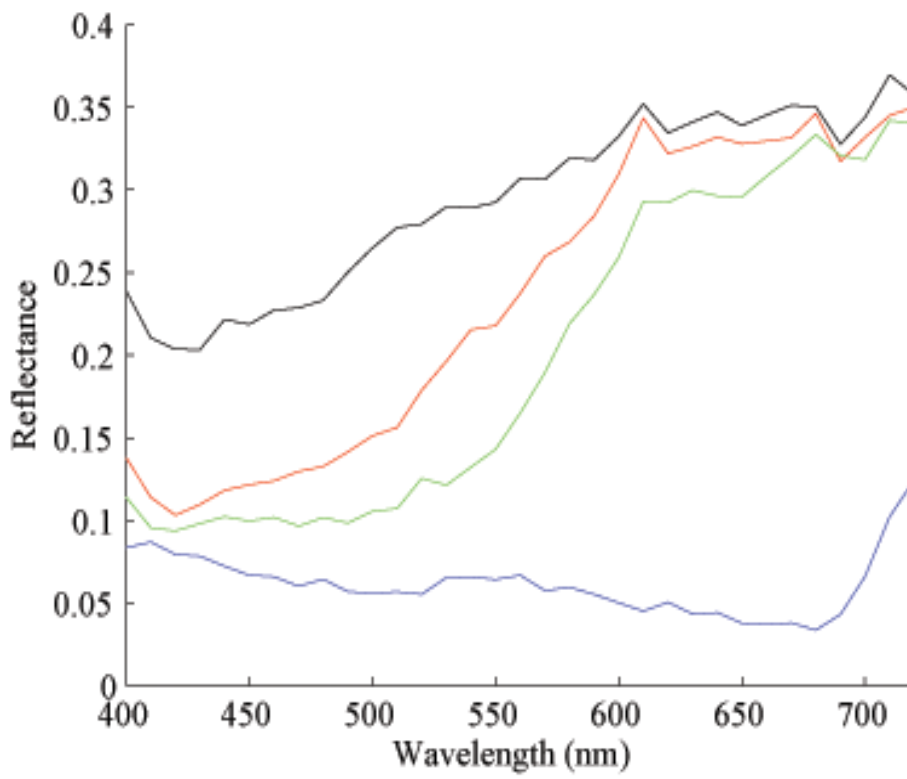
The database described in [4] consists of 50 close-up and distant images of a great variety of urban and rural scenes from the Minho region of Portugal. These images were recorded in sunlight without clouds or under a sky with uniformly distributed clouds.

The acquisition system used is based on a low-noise Peltier-cooled digital camera providing a spatial resolution of 1344×1024 pixels with a tuneable liquid-crystal filter in front of the lens. Immediately after acquisition, the spectrum of light reflected from a small neutral (Munsell N5 or N7) reference surface in the scene is measured using a telespectroradiometer. The effective spectral reflectance at each pixel is computed normalizing the signal against that obtained from the reference surface. For more details on the acquisition procedure, the reader is referred to [4].

In Figure 4 (a) we can see the image from the database that we selected for our experiments. It also shows (in the centre of the coloured circles) the pixels considered. The reflectance spectra of the 4 points are shown in Figure 4 (b).



(a)



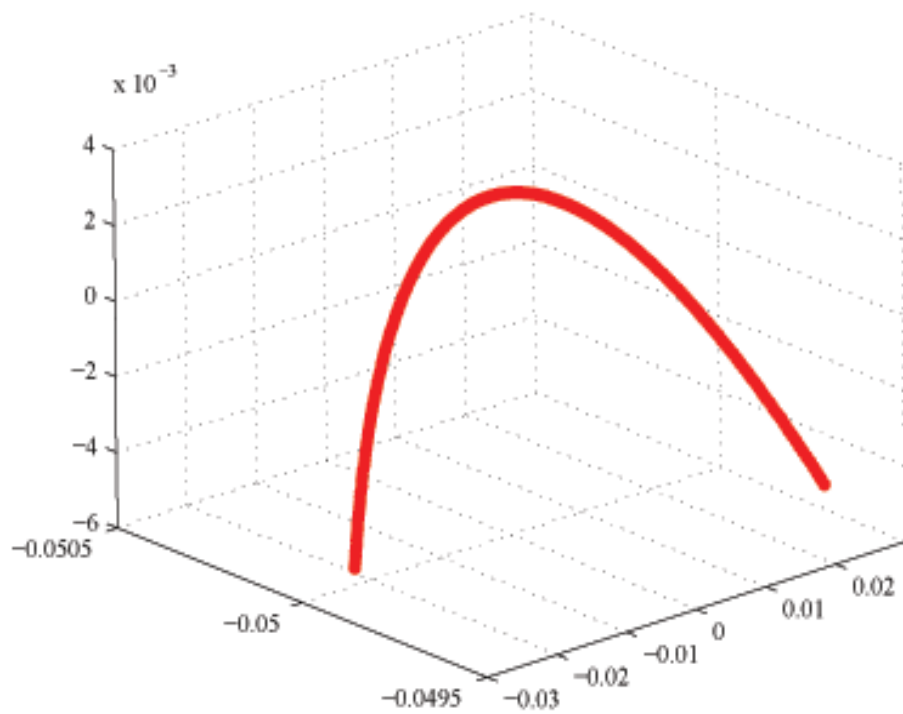
(b)

Fig. 4. (a) Image of the Minho region in Portugal and the four selected pixels, (b) Reflectance spectra of the four points in (a)

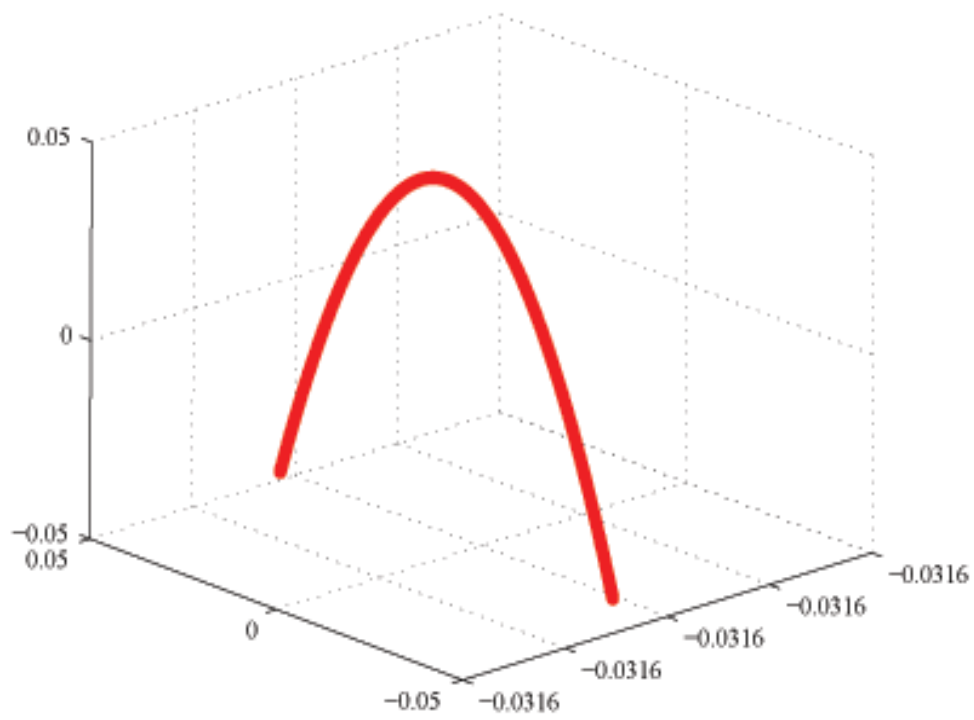
Based on these four selected points in the image we generate four sequences of color signals by pointwise multiplying these reflection spectra with the daylight approximations described in Section 2.2.

3. Experimental Results and discussion

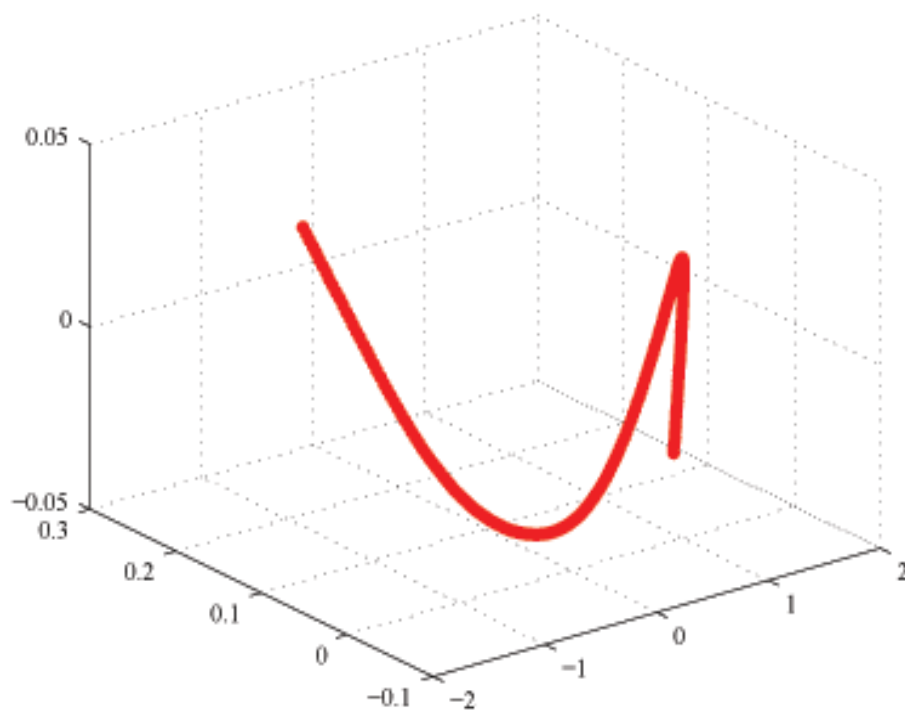
In Figure 5 we show the first three components of the result of applying *PCA*, *LE*, *CCA* and *ISOMAP* to a series of 200 blackbody spectra defined by Eq. 1 in the range from 3000K to 15000K and in the wavelength interval 400nm to 800nm in 1nm steps. As we can see, the result is a parabola-like curve in the first two graphs. This structure is also obtained for parts of the temperature range when using *CCA* and *Isomap*.



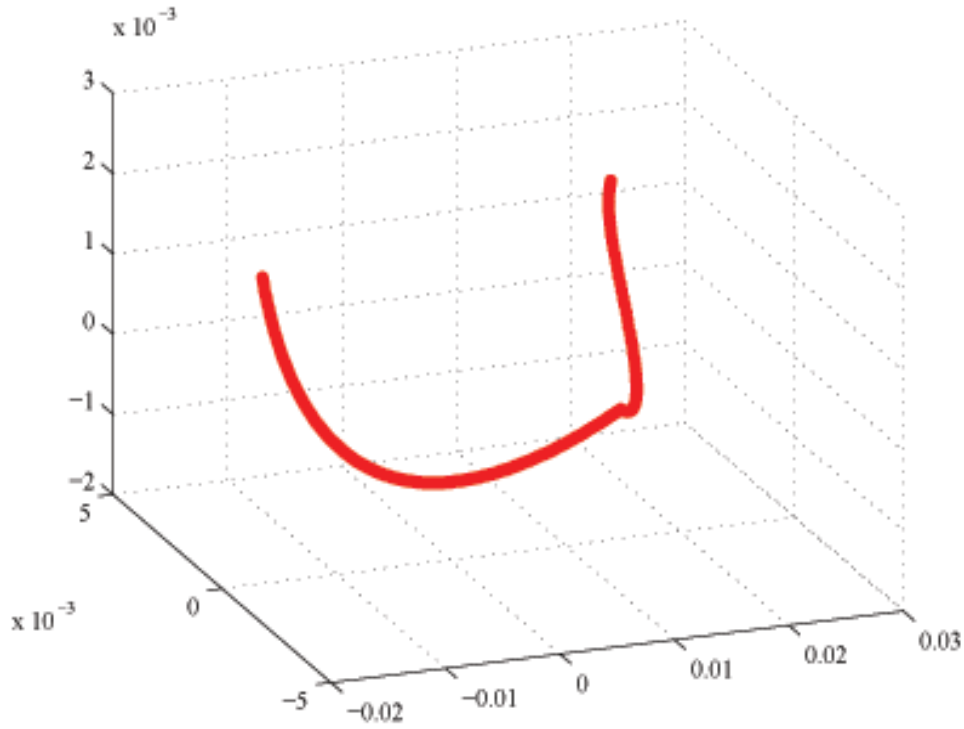
(a)



(b)



(c)

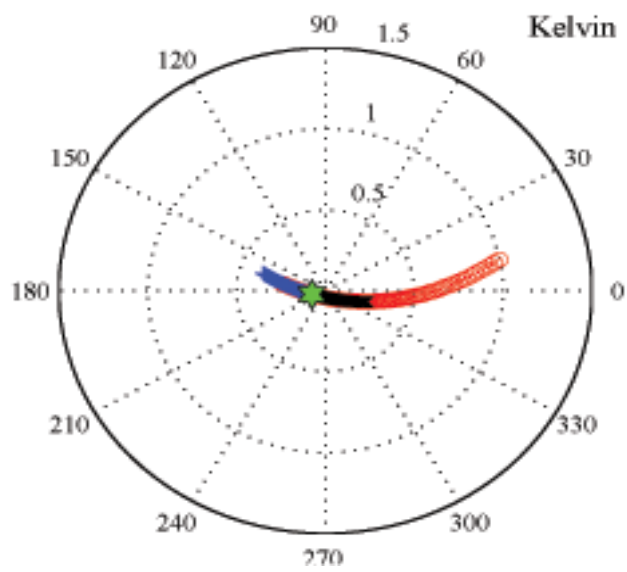


(d)

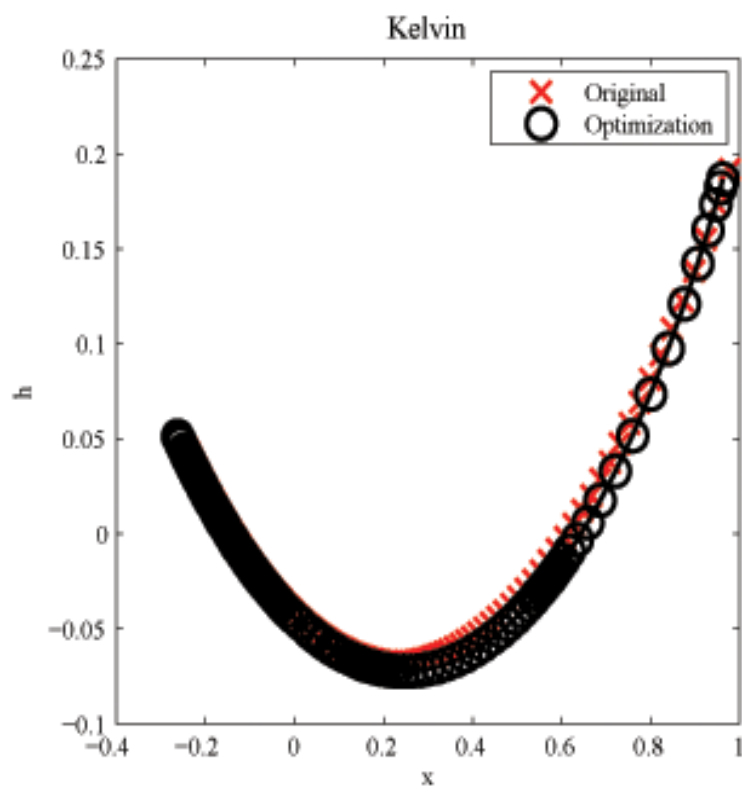
Fig. 5. Analysis of the blackbody radiator spectral series (a) *PCA*, (b) *LE*, (c) *CCA* (d) *Isomap*

The group theoretical analysis of the blackbody radiators is shown in Figure 6. In this figure and the other following figures illustrating the group theoretical method we will show the results of two experiments: In the first experiment we estimate one value of the curve parameter that defines the distance between neighbouring points. In the second experiment we allow different distances between neighbouring pairs and we find these distances by an optimization process. We refer the reader to the appendix for a more detailed description of the underlying framework and the precise definition of these distance values.

In Figures 6(a) and (b) we show the result when the original spectra were selected by equal sampling in the temperature (K) parameterization and in Figure 6(c) and (d) we show the corresponding results for the case when the spectra had equal spacing in the mired ($1/K$) sampling. In Figure 6(a) and (c) we show the equal distance estimation and in Figure 6(b) and (d) the optimized distance estimation.



(a)



(b)

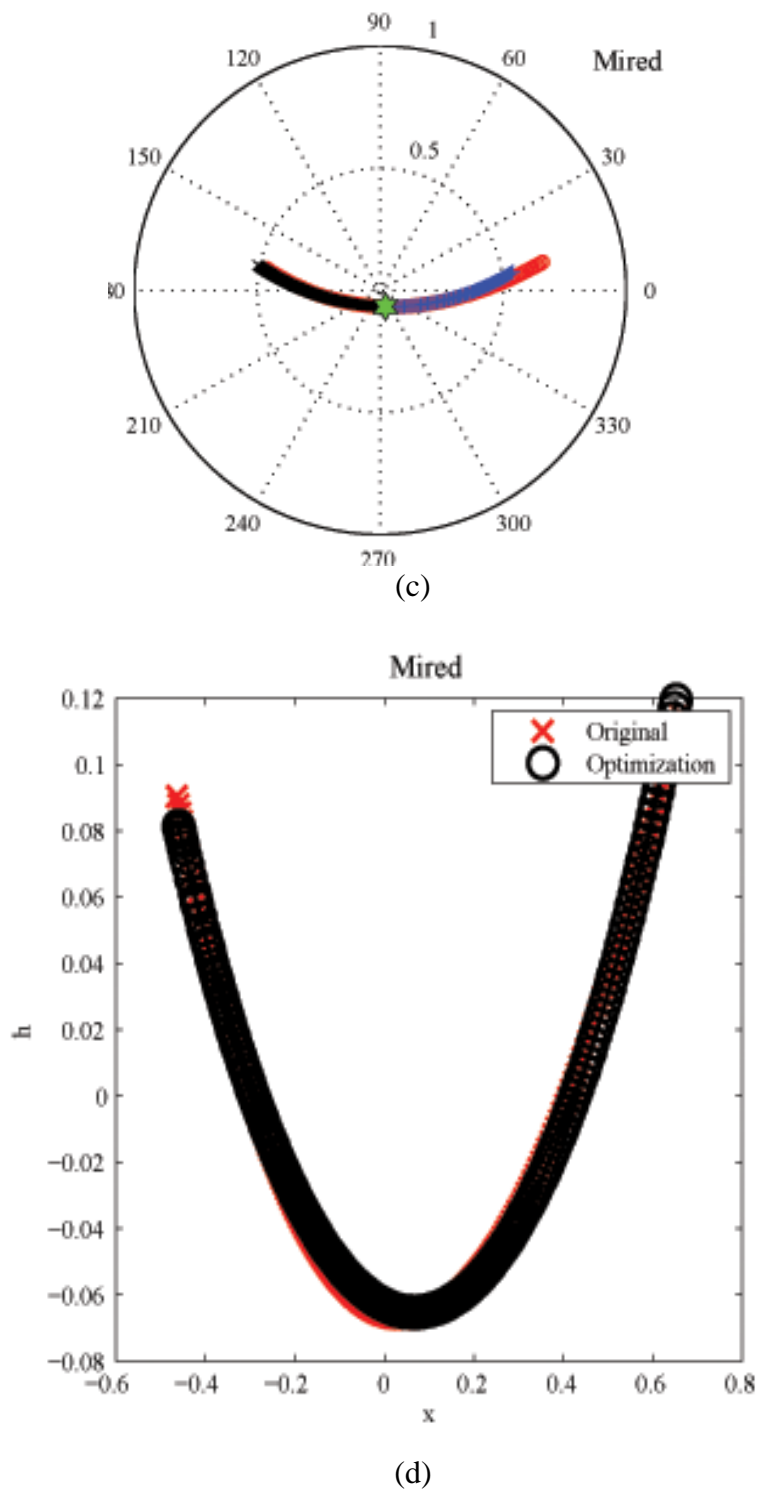
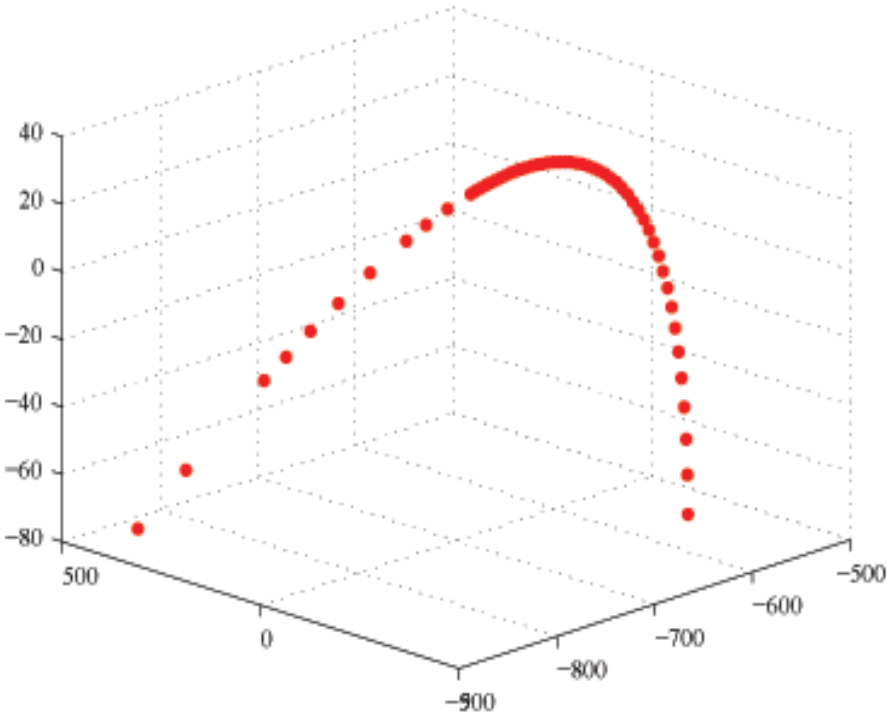


Fig. 6. Group theoretical analysis (a) Sampling in K , equal distance (b) Sampling in K , optimized distances (c) Sampling in $1/K$, equal distance (d) Sampling in $1/K$, optimized distances

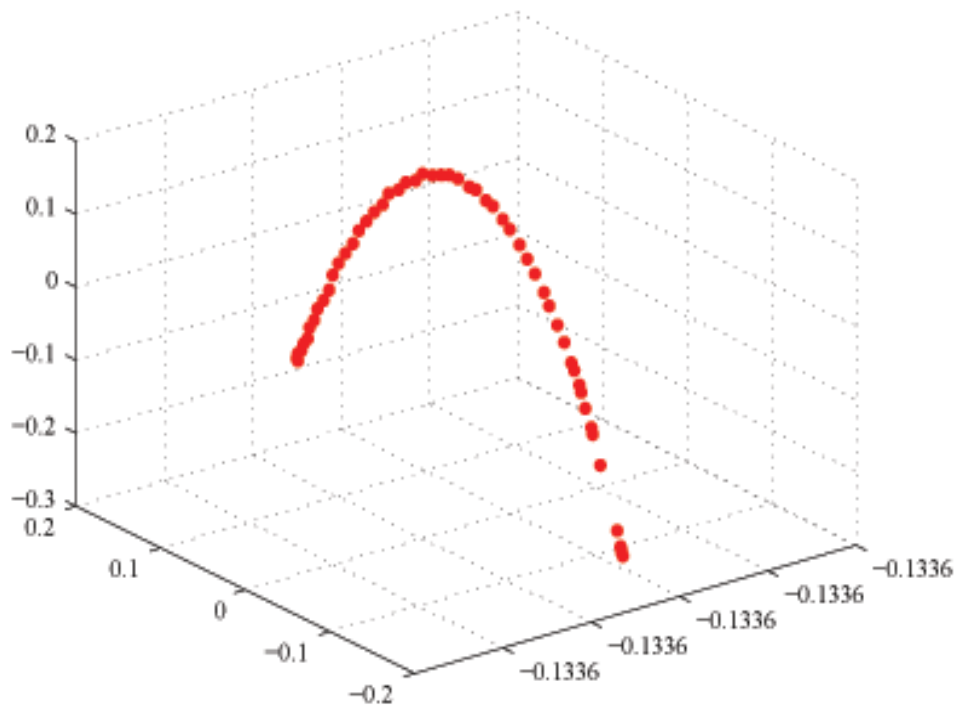
In Figure 6(a) and (c) we mark the start point of our estimation with the star-like symbol which in this case is located at the position of the middle (100st) spectrum in the sequence. We then track the changes backwards (lower temperature) and forward (higher temperatures). We find that all measured points lie on one curve. We also see that the curve parameterization

and the location of the measurement points is in much better agreement for the mired selection than for the temperature parameterization. In Figure 6(b) and (d) we mark original points and estimated points by circles and crosses and see that they are in good agreement both in the temperature and the mired case. We conclude that the location of the points on the unit disk can be described by a hyperbolic curve and the mired parameterization of the blackbody radiators is in good agreement with the curve parameterization given by the $SU(1,1)$ group.

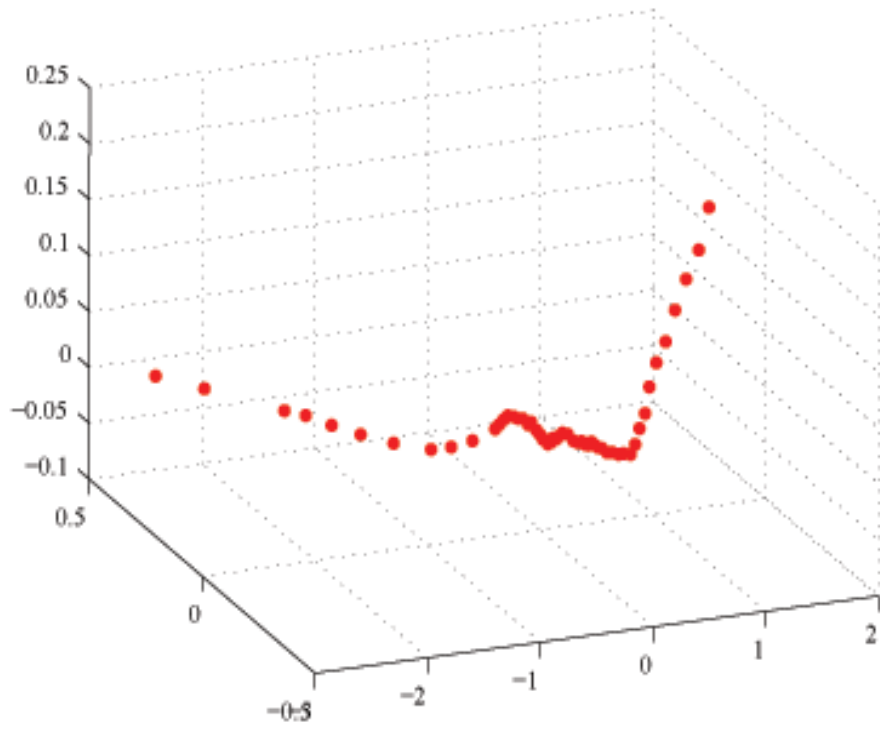
In Figure 7 we can see the 3D representation of the *PCA*, *LE*, *CCA* and *ISOMAP* decomposition of a group of 56 *D*-type daylight spectra. We used temperatures (in Matlab notation) (4000:100:8500)K, (9000:500:10000)K, (11000:1000:15000)K, 20000K and 25000K. Also in this case *PCA* and *LE* results have a smooth shape behaviour (as in Figure 5), which is not the case for *CCA* and *ISOMAP*.



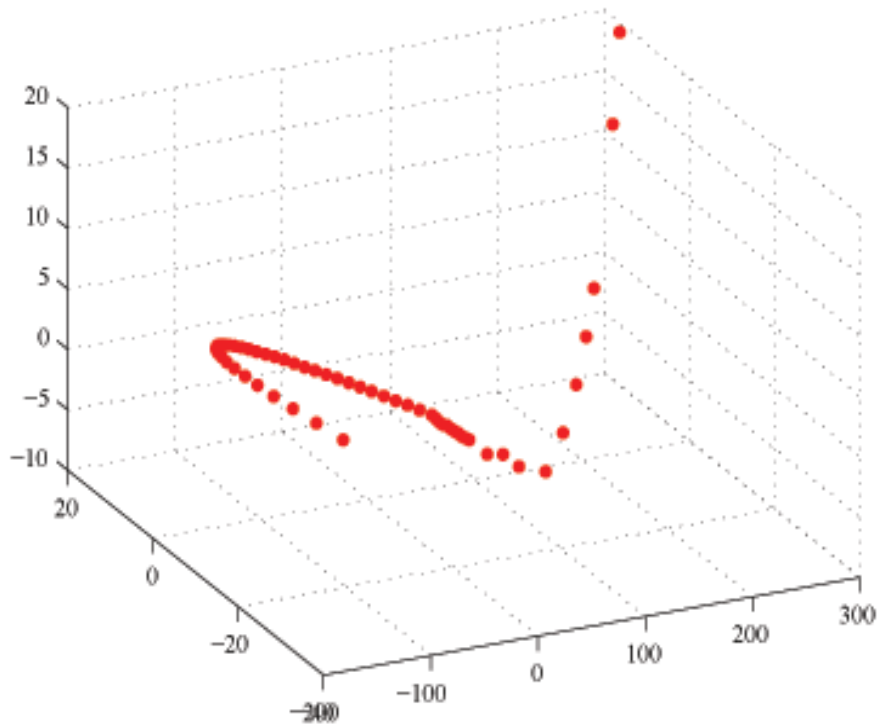
(a)



(b)



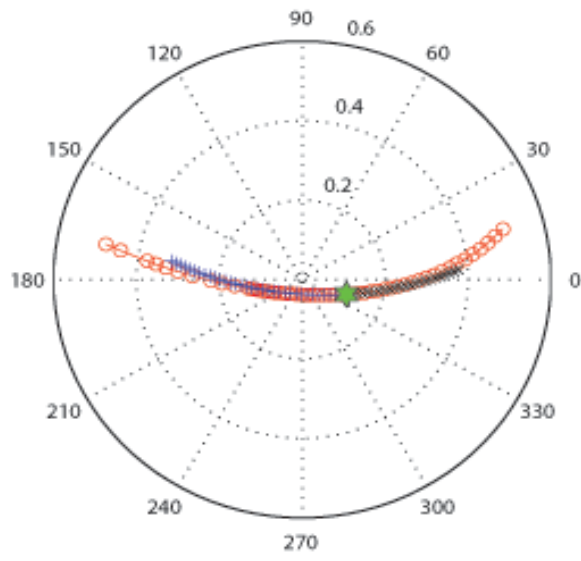
(c)



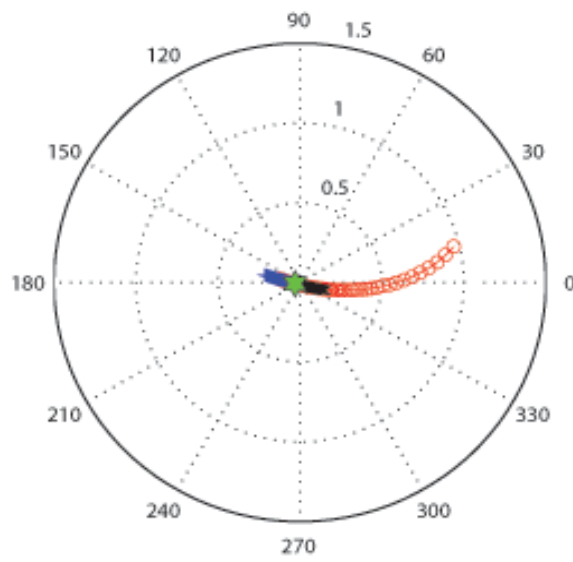
(d)

Fig. 7. Analysis of D -type spectra using (a) PCA , (b) LE , (c) CCA , (d) $ISOMAP$

In Figures 8 and 9 we show some results obtained by applying the hyperbolic geometry-based estimation to the D -type database of daylight approximations. We show again two series of results: The first series is based on the fixed-step assumption of spectral change and the second series estimates optimal step lengths between the samples. Each of these series consists of three figures: the first investigates the spectra introduced in Section 2.2. The other two series consist of approximations in a linear and mired sampling of the same temperature interval as in the original sequence. The spectra in these series are derived from this original sequence by interpolation. Each sequence consisted of 100 spectra.



(a)



(b)

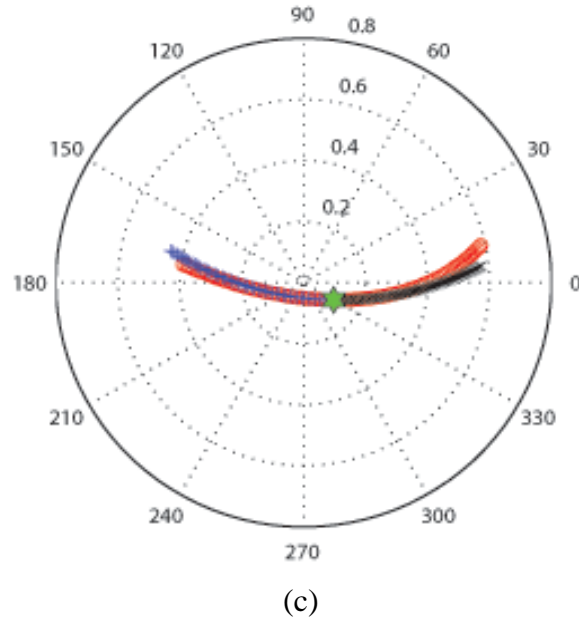
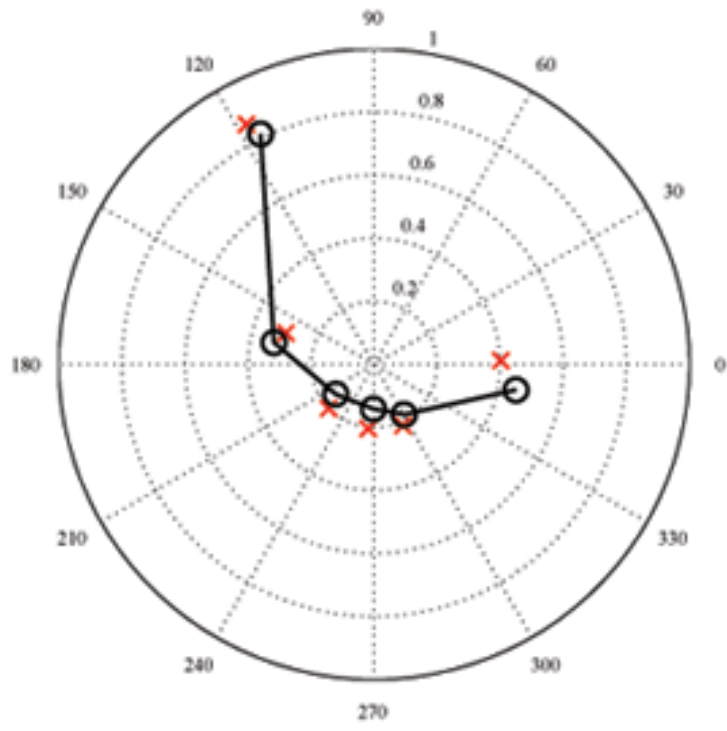
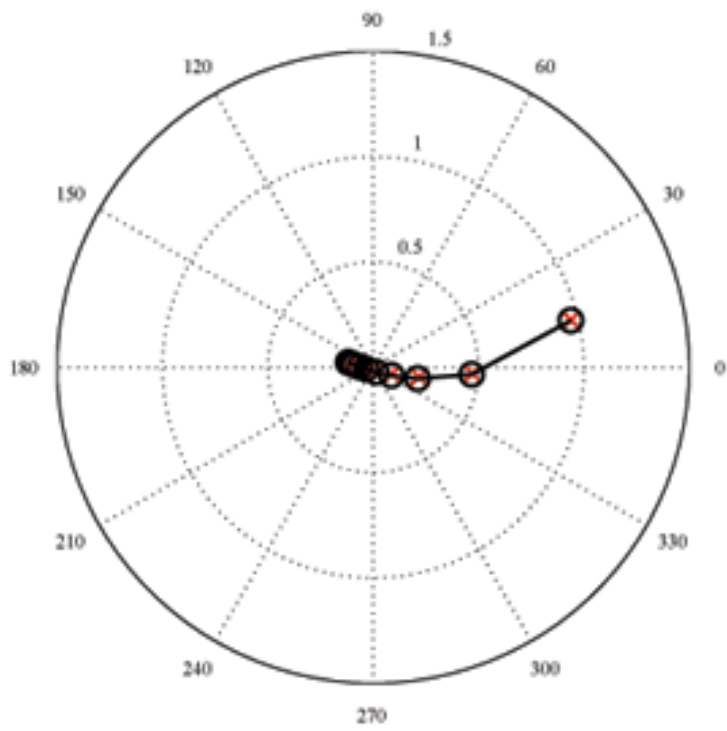


Fig. 8. Position of coefficients on the unit disk. Solid dots original coefficients and (o) estimated by Lie-estimation with fixed step length (a) Original sequence (b) Linear temperature scale (c) Mired temperature scale

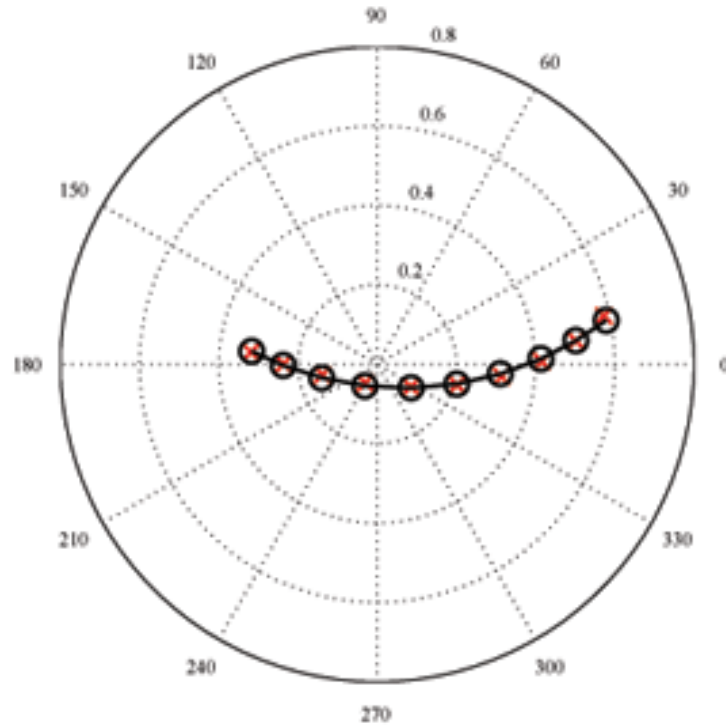
In Figure 8 we show the location of all 56 points in the sequence whereas we plot every 10th point in Figure 9. In Figure 8 we mark with a star the point where we start the tracking of the points in the sequence. The locations of the original points are marked with circles and the locations of the approximations with crosses. We see that the curve fitting is good in the middle of the first sequence whereas the distribution is asymmetric in the second sequence (temperature sampling). We get the best results for the third sequence (mired sampling). From this result we draw the conclusion that also for this database the mired parameterization of the daylight spectra is very similar to the fixed increment version of the group theoretical estimation of the illumination changes.



(a)



(b)



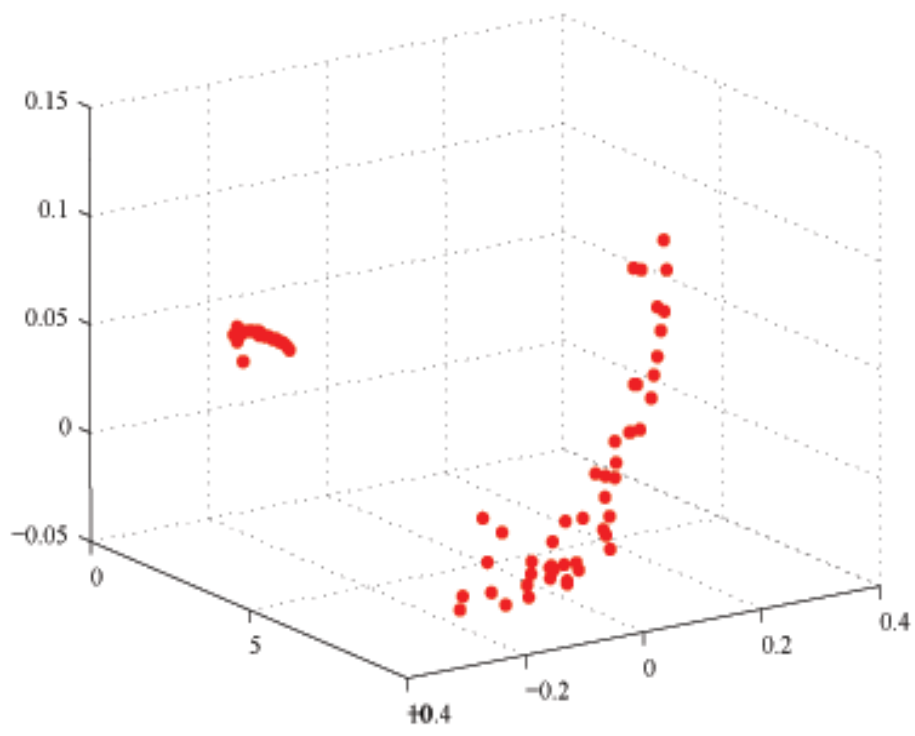
(c)

Fig. 9. Position of coefficients on the unit disk, optimized step length, every 10th sample shown. Solid dots original coefficients and (o) estimated by Lie-estimation with fixed step length (a) Original sequence (b) Linear temperature scale (c) Mired temperature scale

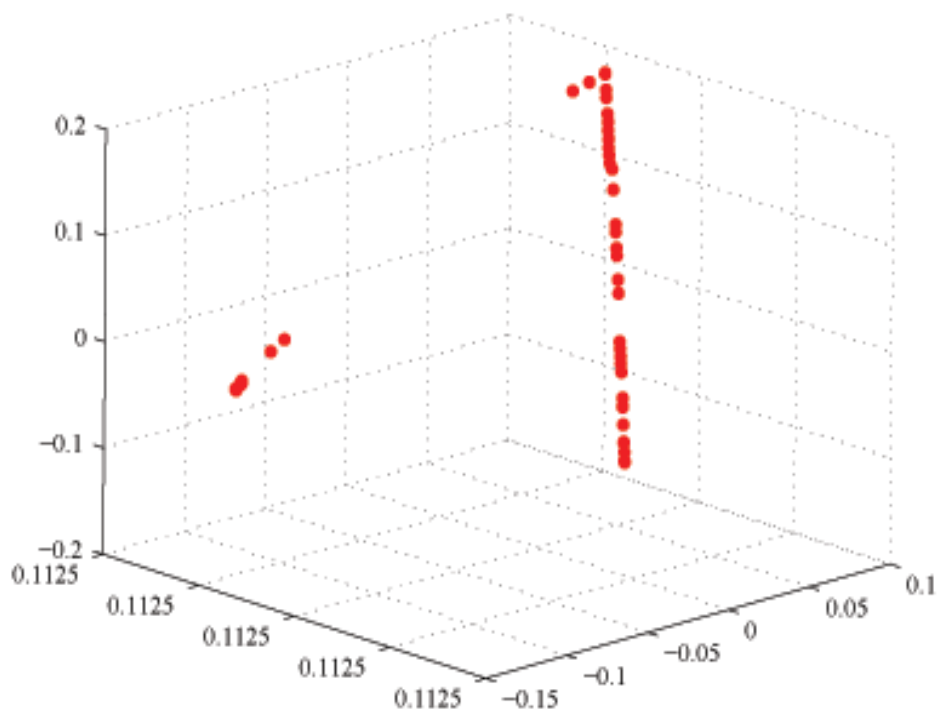
In Figure 9 we use the same sequences as in Figure 8 but now we use optimization of hyperbolic distance errors to find not only one curve but also a good step length distribution along that curve. The results show that in all three cases (original sequence, temperature and Mired sampling) the approximation results are very close to the original data. They also confirm the result from the previous experiment that the step lengths are varying considerably in the original and the Kelvin sampling whereas they are very similar in the Mired sampling.

In the Figure 10 we can see the result of the application of *PCA*, *LE*, *CCA* and *ISOMAP* decomposition to the group of spectra measured on 10th March 1993, that belong to the database of 21871 spectra. This was the longest sequence of measurements under one day in this database, measured in Norrköping, Sweden.

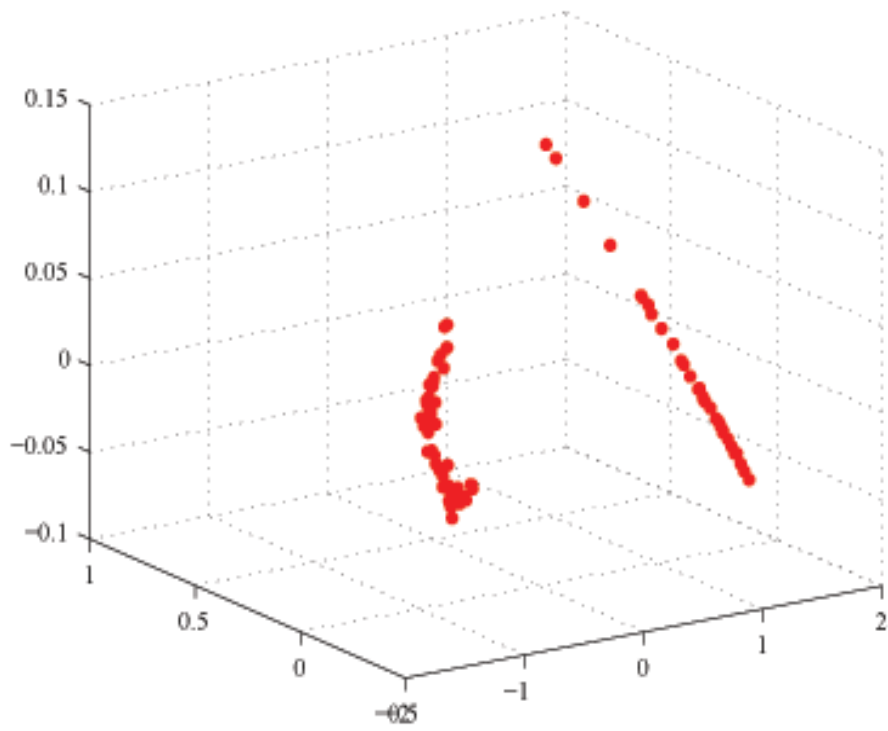
We had for this group of data some matrix singularity problems with *LE*, *CCA* and *ISOMAP*, perhaps because there are only 79 spectra in an 81 dimensional space. Also, and this is applicable to all the data we considered, there are several parameters that must be tuned before we can say that *LE*, *CCA* and *ISOMAP* give reliable results. We tried to use systematic search to find the best parameter values.



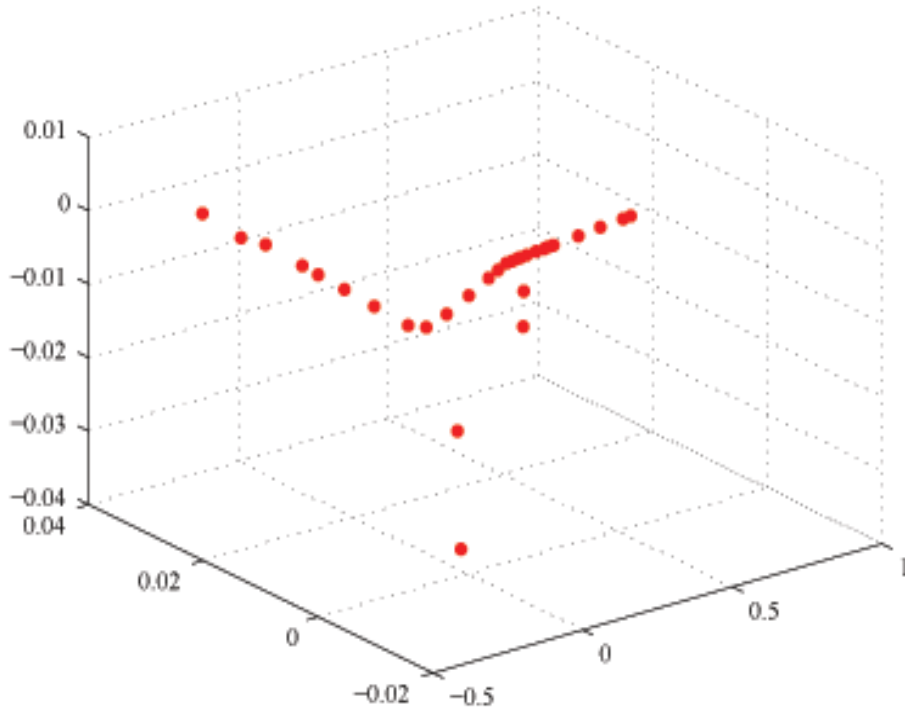
(a)



(b)



(c)



(d)

Fig. 10. Analysis of daylight spectra measured on 10th March 1993 (a) PCA, (b) LE, (c) CCA, (d) Isomap

Figure 11 shows the corresponding estimates for the hyperbolic geometry for the 10th March 1993 spectra, where (a) is the equal step size and (b) the optimal step size approximation. We see that the assumption of a uniform change (shown in (a)) is clearly not valid. Figure 11(b) shows that the optimization gives a good estimate of the point locations. These results confirm the conclusions from the last experiment that constant step length computed from a short subsequence of points (shown in (a)) is too restrictive. It shows also that the introduction of variable step lengths provides a good approximation of the measured positions in terms of the common curve parameter and the variable step sizes.

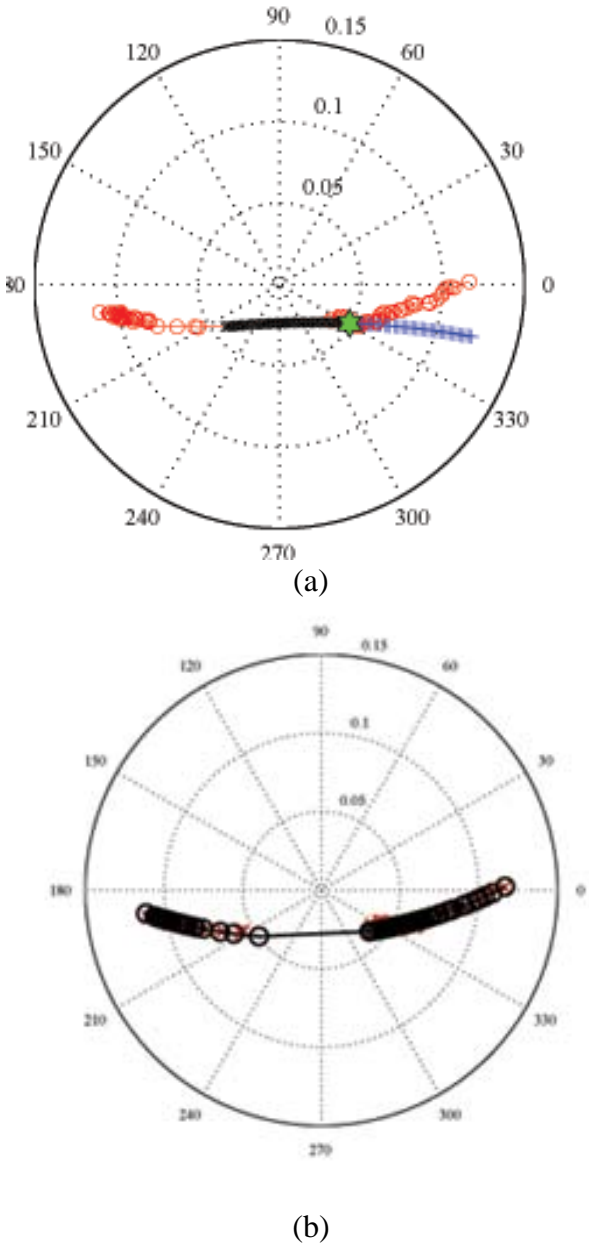
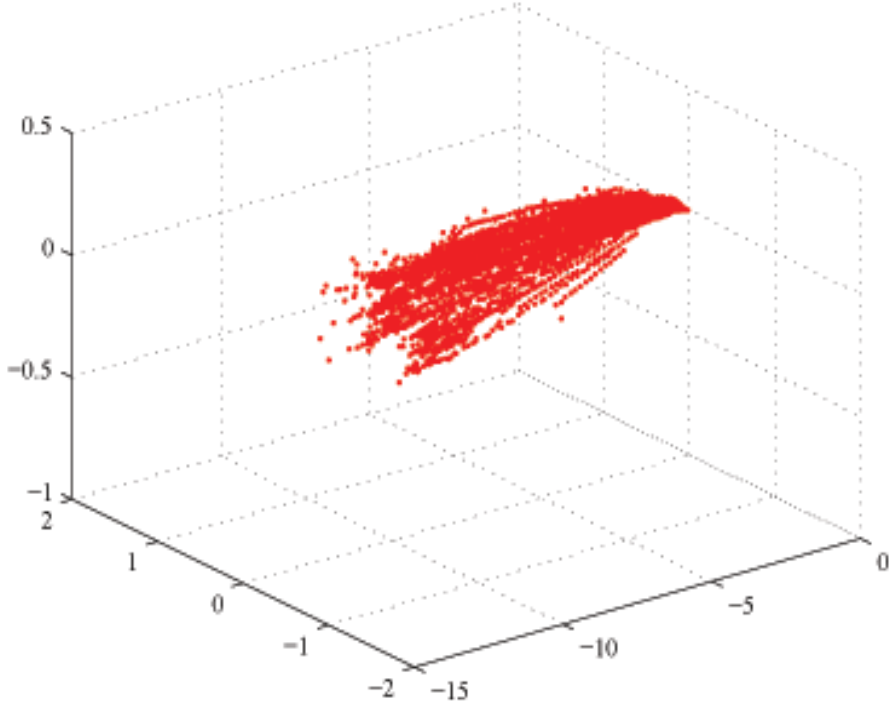
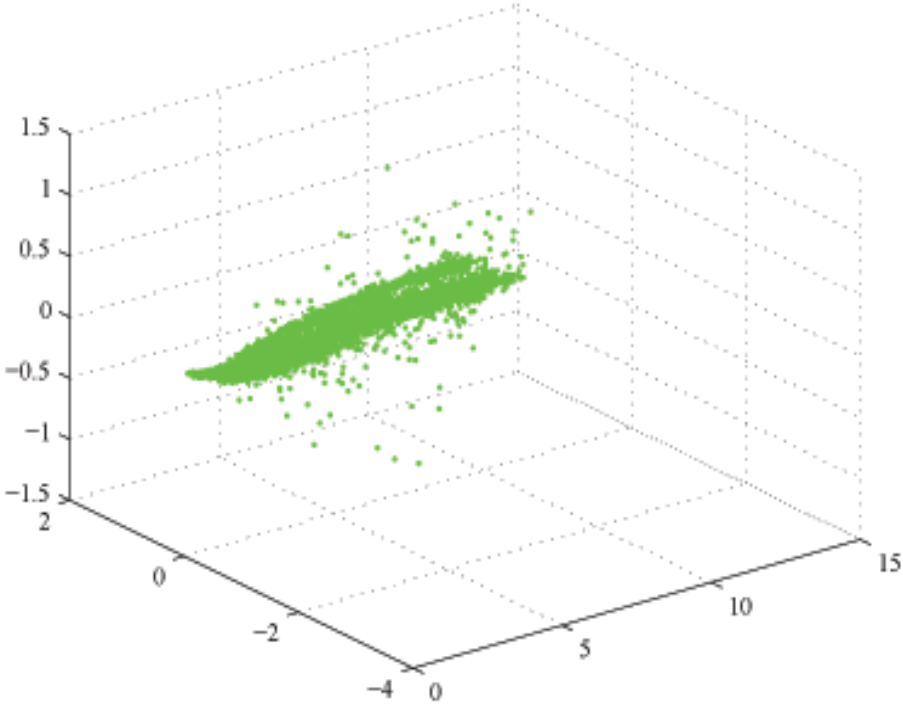


Fig. 11. Estimation of the coefficient series from the measured daylight spectra (a) equal step size (b) optimized step size

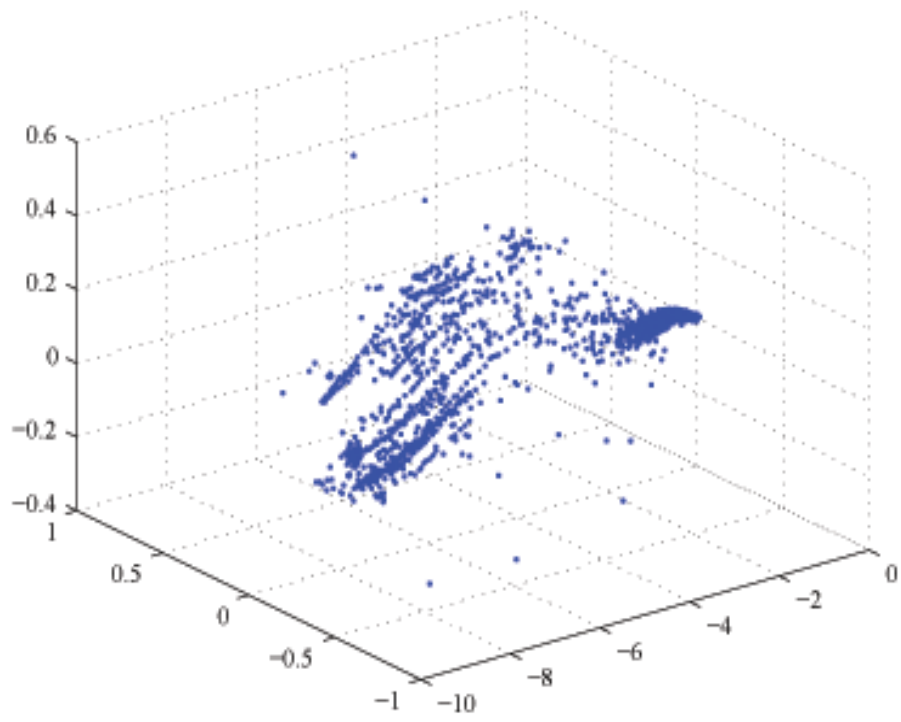
For the next experiment we divided the Swedish Spectra Database of 21871 spectra into four groups corresponding to the four seasons of the year. In Figure 12 we show the result of computing the *PCA* for each group of spectra. These graphs do not seem to show a clear structure in the embedding of the points.



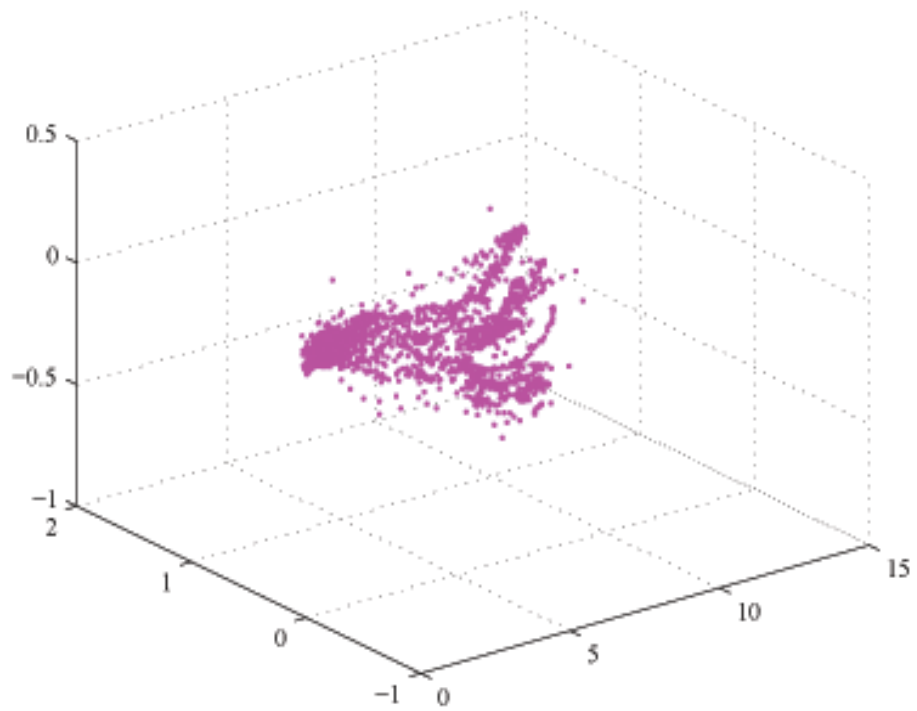
(a)



(b)



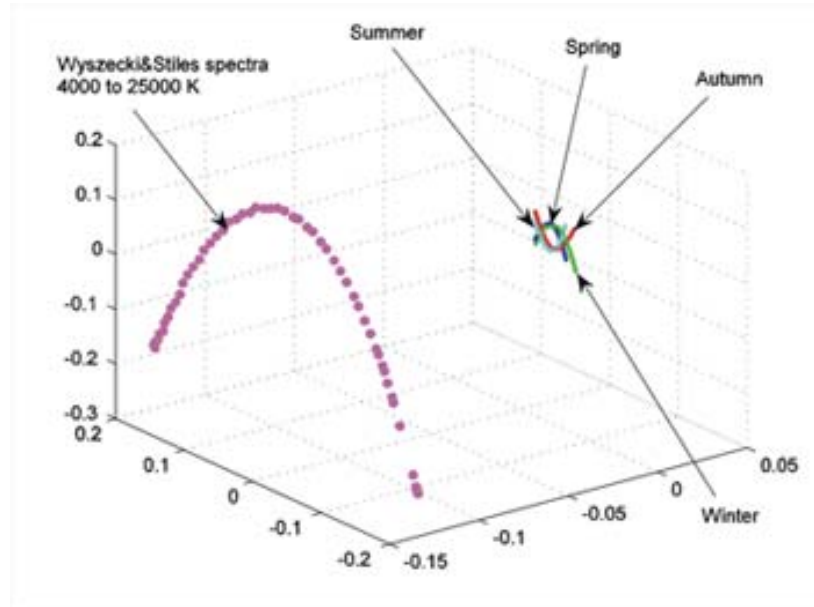
(c)



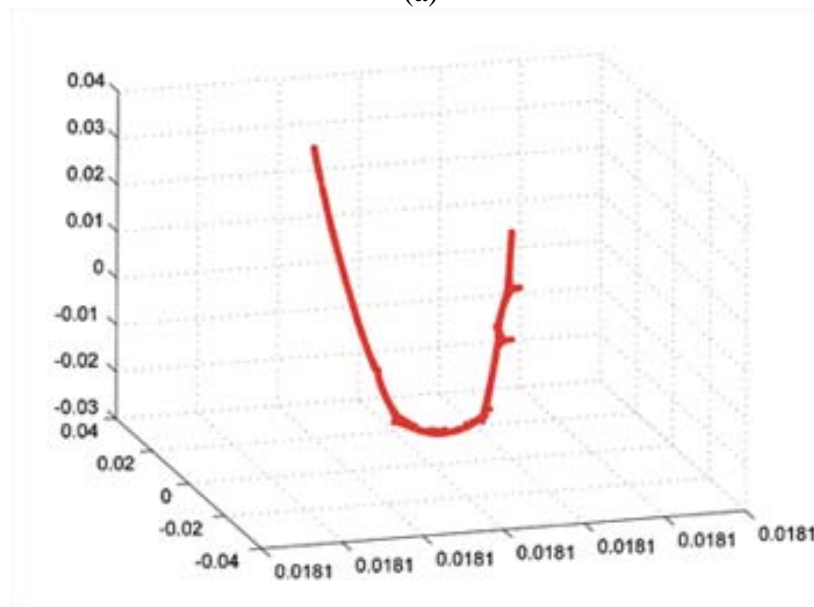
(d)

Fig. 12. *PCA* 3D representation of the seasonal groups of Swedish daylight spectra. (a) Spring, (b) Summer, (c) Autumn, (d) Winter.

We compare in Figure 13 (a), the result of applying *LE* to each group of spectra, and we also represent the shape of the *LE* embedding for the *D*-type spectra of Section 2.2. As we can see in the figure the lower dimensional structure of the seasonally divided spectra and that of *D*-type spectra is similar. In Figure 13 (b) we show a *zoomed* version of the 3D representation for the *Autumn* group.



(a)



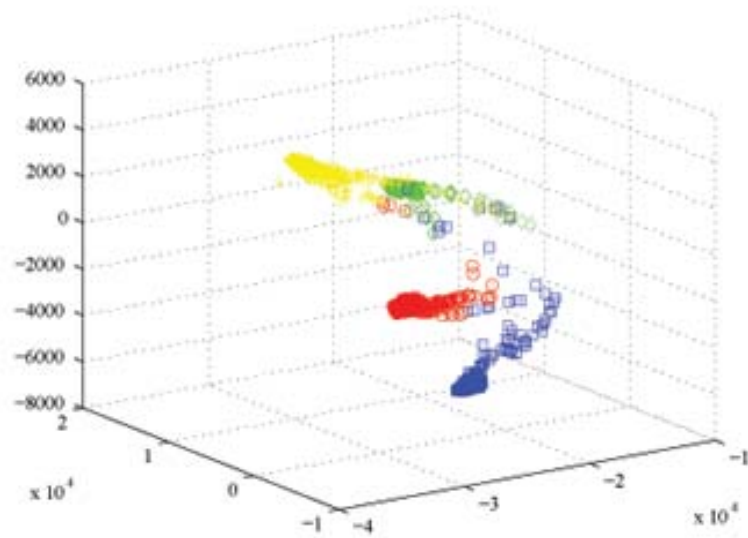
(b)

Fig. 13. (a) *LE* result for the seasonal groups of the Swedish spectra, together with the *D*-type spectra approximation, (b) *Zoomed* representation of the *Autumn* group of data

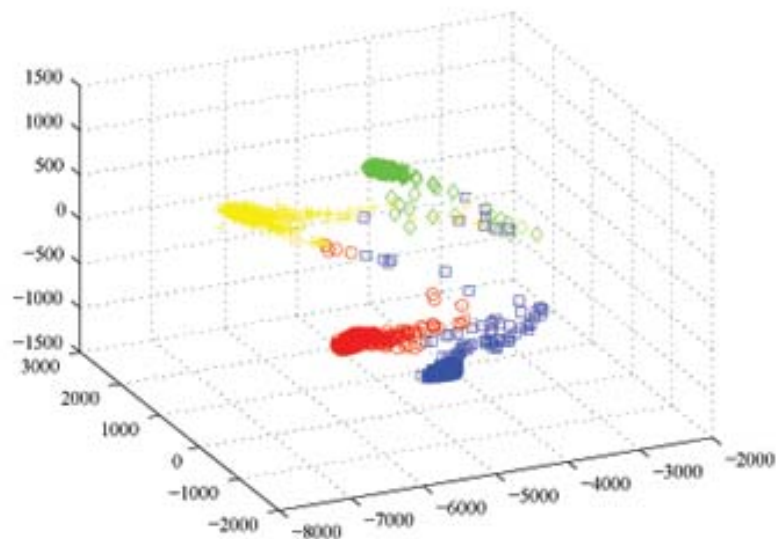
In Figure 14 we show the *PCA* result on the group of 26 images of four wooden toys, each one of the 26 using an illuminant with a different spectral distribution. For these images we investigated two different representations of the measurements. In a first experiment we took

3 of the 26 Images and applied *PCA* on each image separately (a random selection of 10% of the pixels, being the same for the 3 Images). Vectors live here in a 33 dimensional space. We found that the 3 dimensional *PCA* representation of the 3 Images has the same structure. In Figure 14 we only plot the results of one of them.

In a second experiment we created for each one of the 10% of the pixels selected an extended vector made by the addition in the same vector of the spectra of that pixel in each one of the 26 Images (and then we obtain for each pixel a vector in a $33 \times 26 = 858$ dimensional space). We applied *PCA* to investigate the 33 dimensional spectral space and also the 858 dimensional space. It seems (see Figure 14) as if the *PCA* does not have the ability to discover changes in the structure of the distribution of points due to changes in illumination conditions.



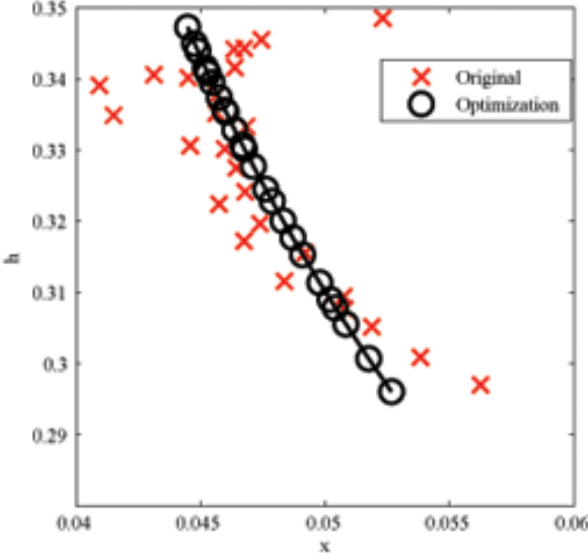
(a)



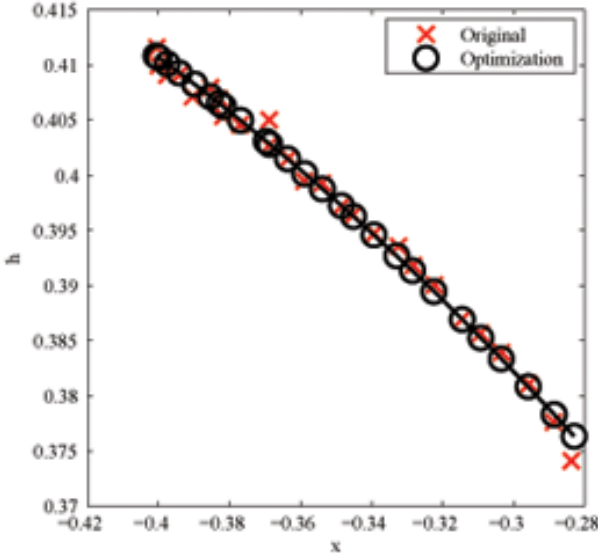
(b)

Fig. 14. (a) *PCA* result on the 858 D space for the 26 images of the 4 wooden toys, (b) *PCA* result on the 33 D space. In (b), the result for 1 of the 3 selected Images is shown.

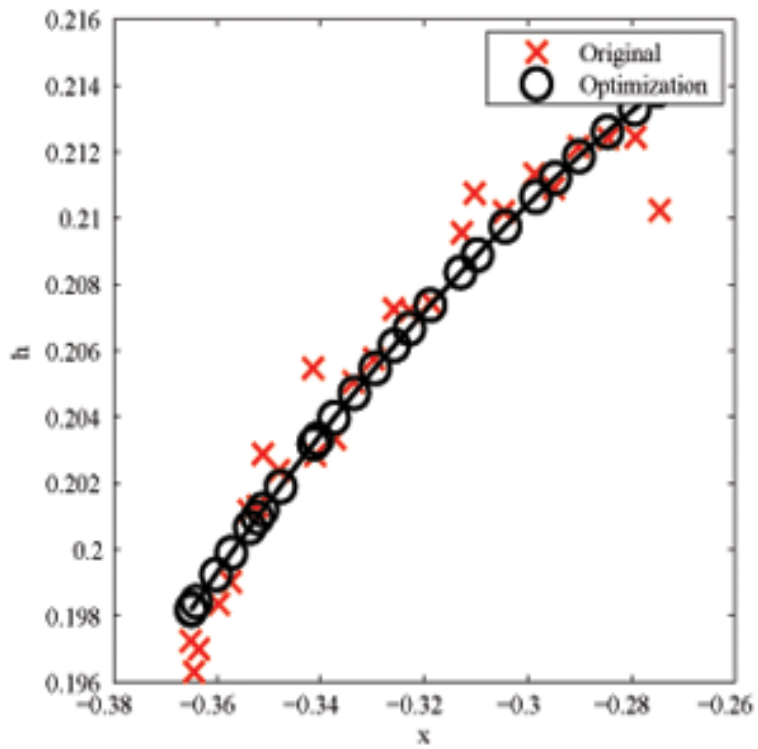
For the application of the hyperbolic geometry-based estimation to this group of 26 images, we averaged first the real and imaginary parts of the chromaticity descriptors (see the appendix for a more detailed description) along a column in each of the four wooden toys that form the image. Then we estimated again the curves and optimal step lengths. The results are shown in Figure 15 and they show that for the three rightmost regions the result is very good whereas it is less satisfactory for the leftmost toy.



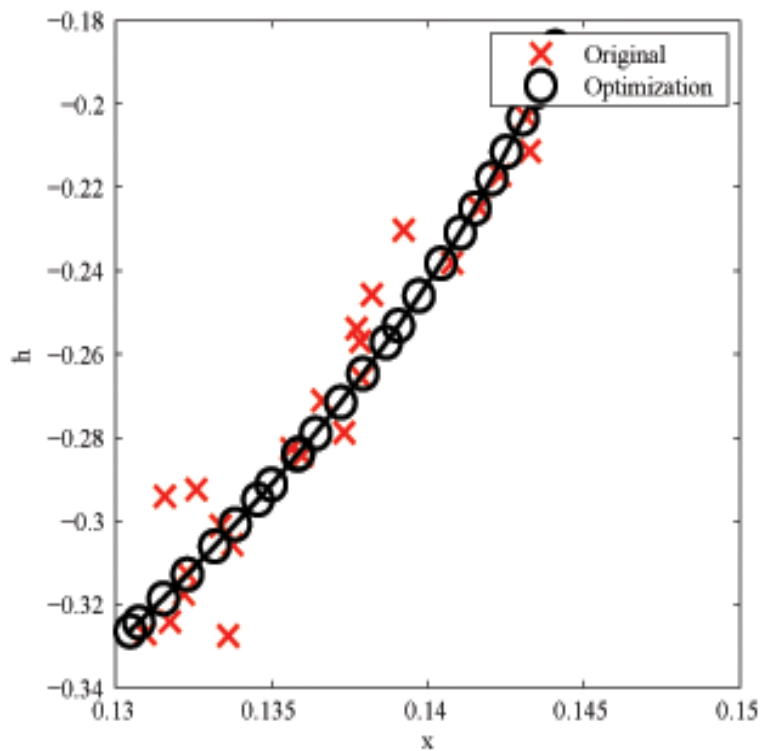
(a)



(b)



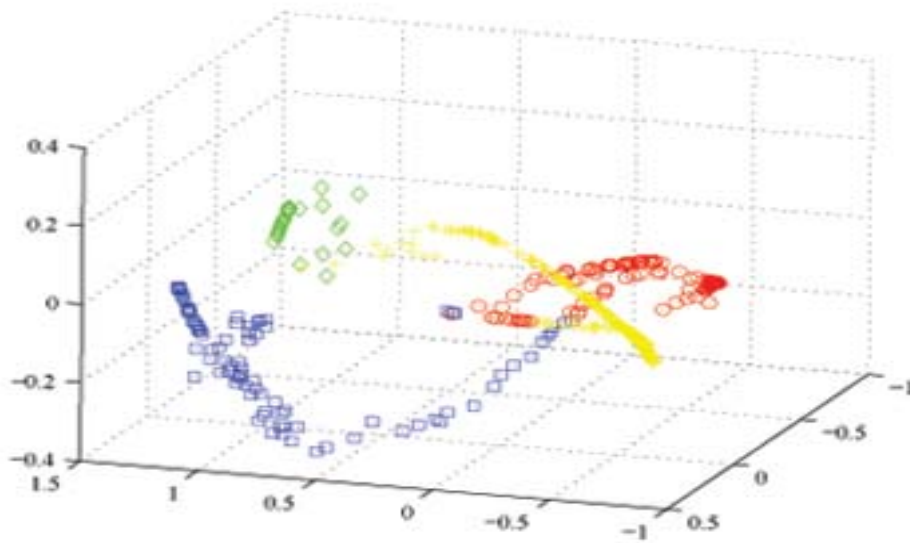
(c)



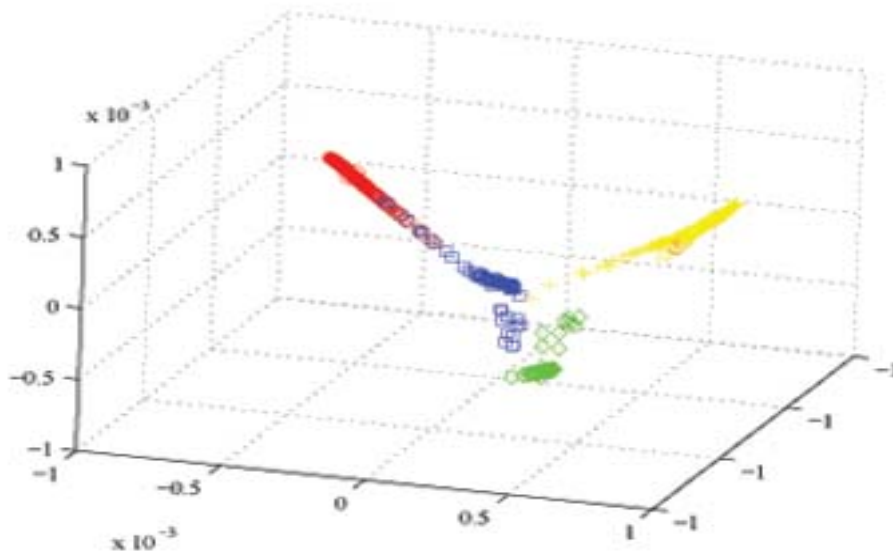
(d)

Fig. 15. Estimation of the coefficient series from four columns in the toy image (a) leftmost column, (b) second column from left, (c) third column from left (d) rightmost column

In Figure 16 we show the results of the application of *CCA* on a random selection of a 10% of the pixels of the wooden toys images in the 33 and 858 dimensional spaces, with the same procedure as that explained for *PCA*.



(a)



(b)

Fig. 16. (a) *CCA* for a 10% of the wooden toys image pixels in the 858 dimensional space, (b) *CCA* for a 10% of the wooden toys image pixels of one image in the 33 dimensional space.

There seems to be a change in structure of the 3D embedding due to a change in illumination, though it may be difficult to identify what are the implications of this change in this low dimensional embedding.

For the other methods (*LE* and *ISOMAP*) we could not produce results that showed significant structures in the low-dimensional representations.

The results of the next experiment are shown in Figure 17. In this Figure we show the 3D representation of the *PCA* decomposition of the color signals generated from four points of a multispectral image of a natural scene [4] (those in the middle of the circles of Figure 4(a)) and the sequence of daylight spectra described in connection with Figure 2(a).

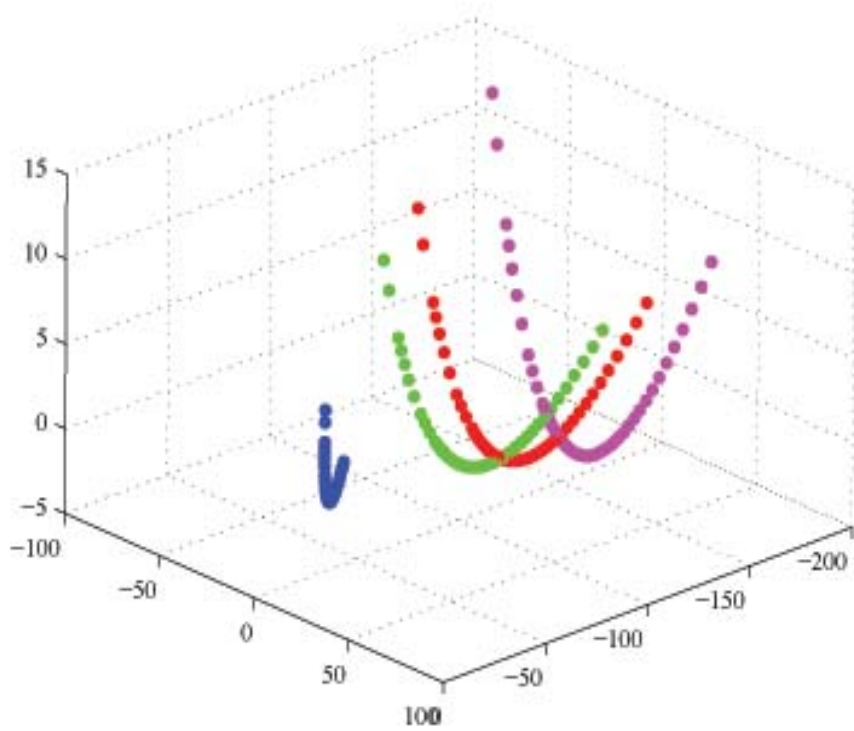
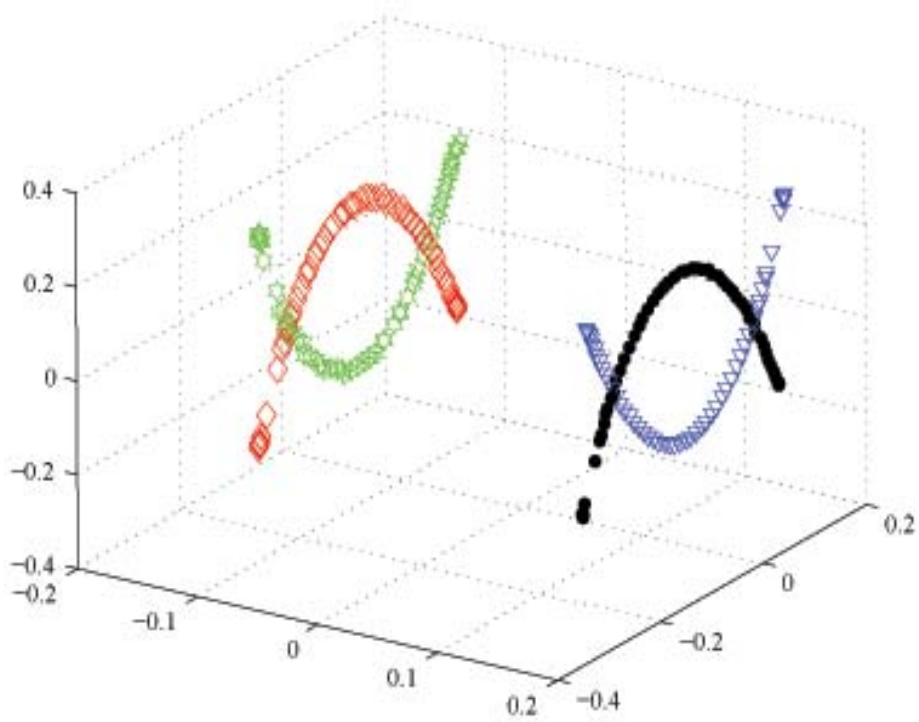
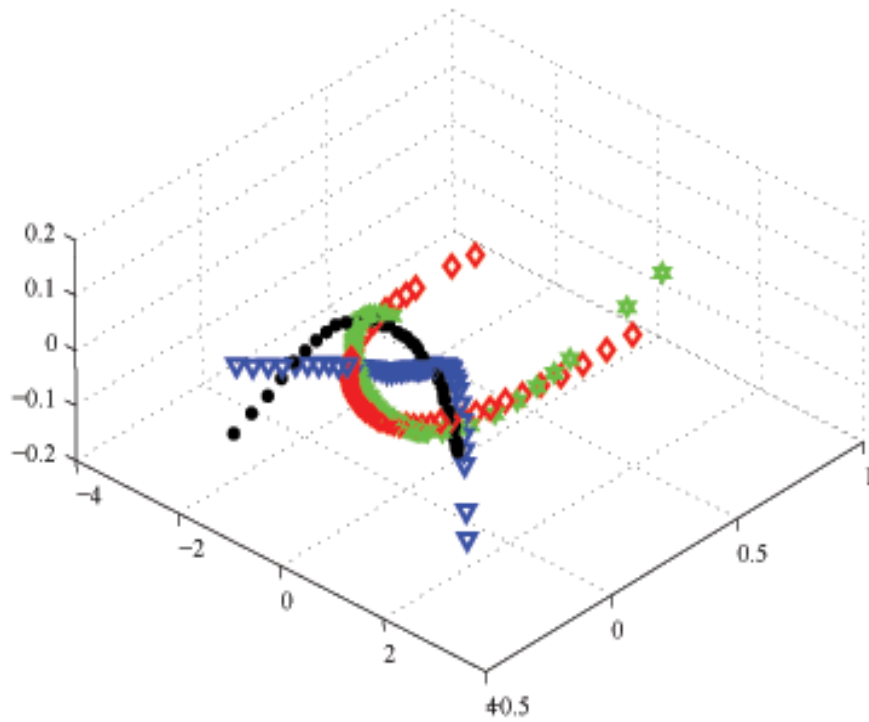


Fig. 17. *PCA of four points of a multispectral image of Minho natural scene database.*

In Figure 18 we show the representation obtained by application of *LE* and *CCA* to the four sequences of color signals.



(a)

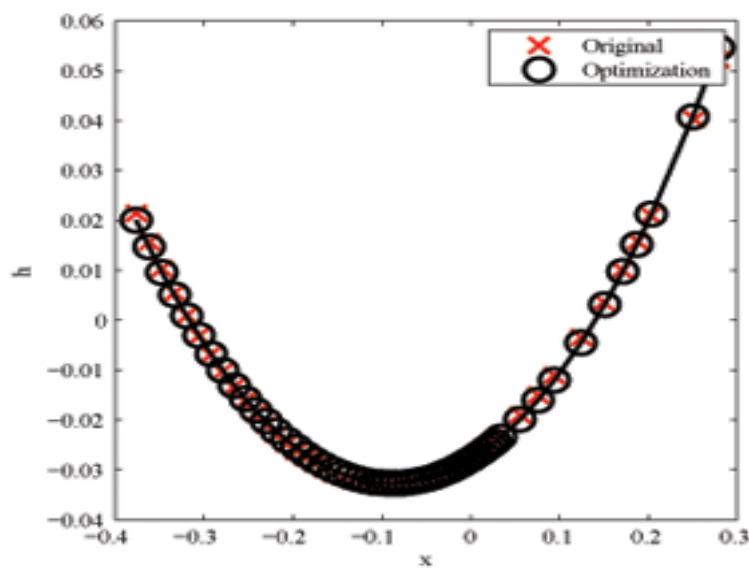


(b)

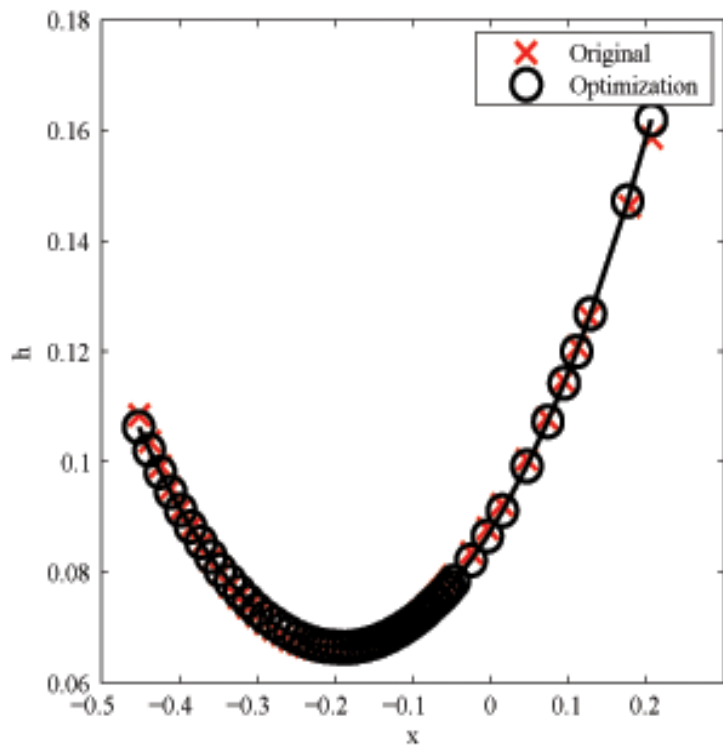
Fig. 18. (a) *LE* for four color signal sequences for one of the Images of the Foster database, (b) *CCA* for the same sequences

We can also see in Figures 17 and 18 the parabolic form of the curves for each one of the four points in the image, though it is not so clear for *CCA*.

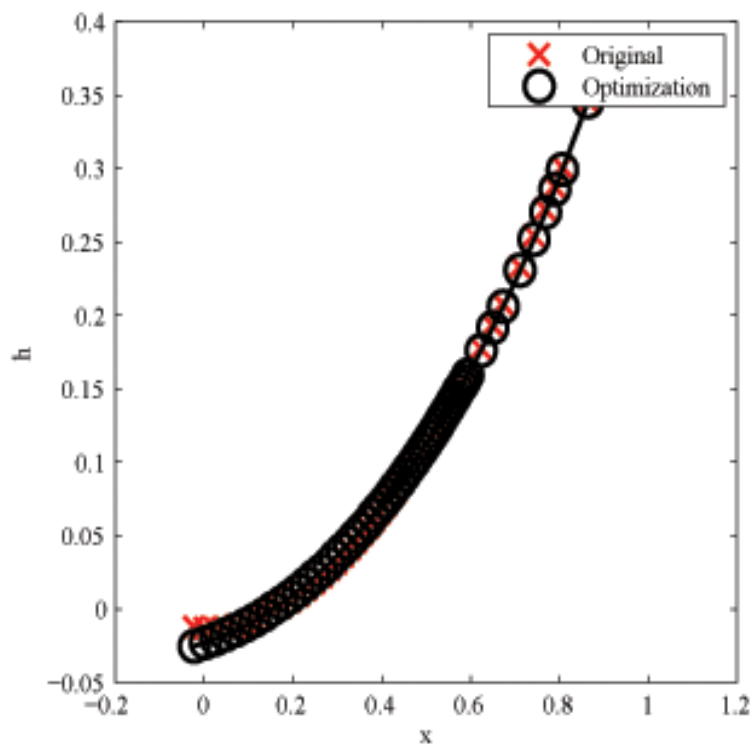
Figure 19 shows the result of using the optimized version of the hyperbolic estimation procedure for these four sequences of color signals.



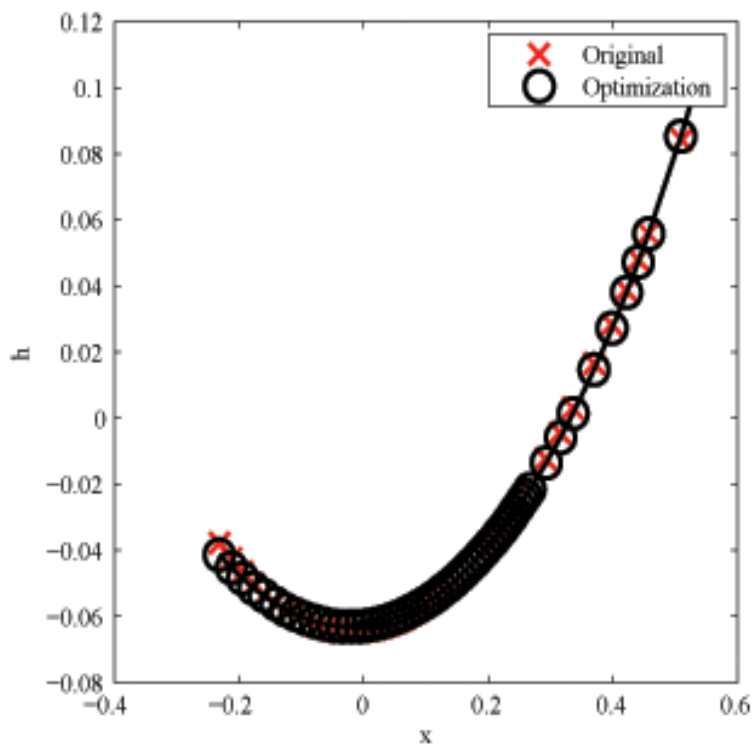
(a)



(b)



(c)



(d)

Fig. 19. Estimation of the coefficient series from four points in a multispectral image of Foster's database under simulated daylight changes

Also here we see that all four sequences are located on hyperbolic curves and that the shape of these curves is characteristic for the different scene points.

4. Conclusions

In this paper we reported our experiments with several dimensionality reduction techniques applied to databases of color spectra. We investigated Principal Components Analysis, Principal Components in relation to group theoretical methods based on hyperbolic geometry, *Laplacian Eigenmaps*, *ISOMAP* and *Canonical Component Analysis*. We applied them to a variety of theoretical, empirically defined and measured spectral datasets.

We found that the conventional *PCA* and the group theoretically derived methods produced results that had a clear theoretical interpretation and the choice of parameters is very easy, essentially to define the number of principal components for *PCA* and to select the parameters for the numerical optimization process used in one variation of the group theoretical estimation.

For the non-linear methods (*LE*, *ISOMAP* and *CCA*) this was much more difficult. Selecting "good" parameters was not easy. Often it was difficult to decide what "good" parameters are and often the simple structure of the output produced was used in this judgement. Another problem with these algorithms is the complex nature of the reduction. It is defined in an abstract framework and very difficult to get an intuitive understanding of the results. Another problem is that these methods produce representations of the data in lower-dimensional spaces but it is very difficult to apply the rule obtained to unknown data vectors that were not part of the original data set.

Apart from that we found that the *Laplacian Eigenmaps* method (*LE*) worked best for most of the data groups (except the group of 26 images of different illuminations of 4 wooden toys,

and the spectra of 10th march 1993 of the 21871 spectra database). The smooth structure of some of the low dimensional representations suggests that those representations may be useful for data compression.

Acknowledgments

This work has been partially funded by the Ministry of Education and Science of the Spanish Government through the *DATASAT* project (*ESP – 2005 – 00724 – C05 – C05*). Pedro Latorre Carmona is a *Juan de la Cierva* Programme Researcher (Ministry of Education and Science). The authors thank Prof. Foster and his group for providing the images of their multispectral database. We thank Prof. Sha, Prof. Saul, Prof. Belkin, and also to Profs. Tenenbaum, de Silva and Langford for making their dimensionality reduction codes accessible via the Internet.

References

- [1] M. Belkin, P. Niyogi. Laplacian Eigenmaps for Dimensionality Reduction and Data Representation. *Neural Computation*, 15(6):1373-1396, 2003.
- [2] V. Bonnardel and L. T. Maloney. Daylight, biochrome surfaces, and human chromatic response in the Fourier domain. *J. Opt. Soc. Am. A*, 17(4):677–686, 2000.
- [3] T. H. Bui. Group-Theoretical Structure in Multispectral Color and Image Databases. Thesis, *Department of Science and Technology Linköping University*, 2005.
- [4] D. H. Foster, K. Amano, S. M. C. Nascimento, M. J. Foster. Frequency of metamerism in natural scenes. *J. Opt. Soc. Am. A*, 23(10):2359–2372, 2006.
- [5] B. Funt, D. Kulpinski, V. Cardei. Non-linear embeddings and the underlying dimensionality of reflectance spectra and chromaticity histograms. In *The 9th Color Imaging Conference: IS&T*, Scottsdale, Arizona, USA, 2001.
- [6] J. Hernández-Andrés, J. Romero, and R. L. Lee Jr. Colorimetric and spectroradiometric characteristics of narrow-field-of-view clear skylight in Granada, Spain. *J. Opt. Soc. Am. A*, 18(2):412–420, 2001.
- [7] J. Hernández-Andrés, J. Romero, J. L. Nieves, and R. L. Lee Jr. Color and spectral analysis of daylight in southern Europe. *J. Opt. Soc. Am. A*, 18(6):1325–1335, 2001.
- [8] R. W. G. Hunt. *Measuring Colour*. Fountain Press, Kingston-upon-Thames, 1998.
- [9] D. B. Judd, D. L. MacAdam, G. Wyszecki. Spectral distribution of typical daylight as a function of correlated color temperature. *J. Opt. Soc. Am.*, 54(8):1031–1040, 1964.
- [10] S. Kawata, K. I. Sasaki, and S. Minami. Component analysis of spatial and spectral patterns in multispectral images .1. Basis. *J. Opt. Soc. Am. A*, 4(11):2101–2106, 1987.
- [11] C. Y. Kuan and G. Healey. Using independent component analysis for material estimation in hyperspectral images. *J. Opt. Soc. Am. A*, 21(6):1026–1034, 2004.
- [12] J. Lehner. *Discontinuous Groups and Automorphic Functions*. American Mathematical Society, Providence, Rhode Island, USA, 1964.
- [13] R. Lenz. Estimation of illumination characteristics. *IEEE Transactions Image Processing*, 10(7):1031–1038, July 2001
- [14] R. Lenz. Spectral color spaces: Their structure and transformations. In *Advances in imaging and electron physics*, volume 138, pages 1–67. Ed. Peter W. Hawkes, Elsevier, 2005.
- [15] R. Lenz and T.H. Bui. Statistical properties of color-signal spaces. *J. Opt. Soc. Am. A*, 22(5):820–7, May 2005.

- [16] R. Lenz, T. H. Bui, and J. H. Andres. Group theoretical structure of spectral spaces. *Journal of Mathematical Imaging and Vision*, 23(3):297–313, November 2005.
- [17] R. Lenz and M. Solli. Lie methods in color signal processing: Illumination effects. In *Proc. ICPR 2006, Hongkong*, volume III, pages 738–741, Los Alamitos, 2006. IEEE-Press.
- [18] J. P. S. Parkkinen, J. Hallikainen, and T. Jaaskelainen. Characteristic spectra of Munsell colors. *J. Opt. Soc. Am. A*, 6(2):318–322, 1989.
- [19] J. Romero, A. Garca-Beltran, and J. Hernández-Andrés. Linear bases for representation of natural and artificial illuminants. *J. Opt. Soc. Am. A*, 14(5):1007–1014, 1997.
- [20] J. Romero, E. Valero, J. Hernández-Andrés, and J. L. Nieves. Color-signal filtering in the Fourier-frequency domain. *J. Opt. Soc. Am. A*, 20(9):1714–1724, 2003.
- [21] K. Sasaki, S. Kawata, and S. Minami. Component analysis of spatial and spectral patterns in multispectral images .2. entropy minimization. *J. Opt. Soc. Am. A*, 6(1):73–79, 1989.
- [22] F. Sha, L. K. Saul. Analysis and Extension of Spectral Methods for Nonlinear Dimensionality Reduction In *Proceedings of 22nd International Conference on Machine Learning* 785–792, 2005.
- [23] G. Sharma. *Digital Color Imaging Handbook*. CRC Press 2003.
- [24] C.L. Siegel. *Topics in Complex Function Theory, Automorphic Functions and Abelian Integrals*. Wiley Interscience, New York, 1971.
- [25] J. B. Tenenbaum, V. de Silva and J. C. Langford. A global geometric framework for nonlinear dimensionality reduction. *Science*. 290:2319–2323, 2000.
- [26] Di-Yuan Tzeng and Roy S. Berns. A review of principal component analysis and its applications to color technology. *Color Research & Application*, 30(2):84–98, 2005.
- [27] S. Usui, S. Nakauchi, and M. Nakano. Reconstruction of munsell color space by a five-layer neural network. *J. Opt. Soc. Am. A*, 9(4):516–520, 1992.
- [28] G. Wyszecki, W. S. Stiles. *Color Science: concepts and methods, quantitative data and formulae*. *Wiley Classics Library*. New York, 2000.
- [29] F. W. Young. Multidimensional scaling. *Encyclopedia of Statistical Sciences*. 5, pp. 649-659, 1985.

Appendix

In this appendix we describe the basic ideas behind the methods we used in our experiments. We follow the description (and notations) of the references mentioned below and we recommend the interested reader to consult these references.

A. Principal Components Analysis

Principal component analysis (PCA) is a mathematical procedure that transforms a number of (possibly) correlated variables into a (smaller) number of uncorrelated variables called principal components. This method aims at reducing the dimensionality (number of variables) of the dataset but retain most of the original variability in the data. The first principal component accounts for as much of the variability in the data as possible, and each succeeding component accounts for as much of the remaining variability as possible. PCA is the standard method used to investigate or compress multispectral data. In PCA methods multispectral vectors containing the measurements from n channels are considered as vectors s in the n -dimensional Euclidian vector space R^n . In this vector space a subspace V of lower dimension m ($m < n$) is constructed such that the orthogonal projection $P: R^n \rightarrow V$ results in minimum mean squared error:

$$\text{mean} \|s - Ps\|^2 \stackrel{!}{=} \text{minimum}$$

where the mean is computed over all relevant vectors s .

This process involves the computation of the eigenvector or Singular Value Decomposition of the data set. For a definition of the Singular Value Decomposition, the reader is referred to [29].

There are two basic variations of PCA, one where the vectors involved are first centered and one where they are used as they are. In the first case the optimal vector space V is spanned by the m eigenvectors of the covariance matrix that belong to the m largest eigenvalues. In the second case the eigenvectors of the matrix containing the second order moments are obtained as solutions instead. In the case where all vectors s assume only non-negative values it can be shown that both approaches usually lead to the very similar results.

B. Basic facts about Lie-theoretical methods

From the non-negativity of the spectral vectors follows that the coefficient vectors of the correlation-based PCA expansion lie in a cone-like subset of the full coefficient space (for the methods of this section of the Appendix we use only the construction based on the correlation matrix). For more details we refer the interested reader to [16,29]). In the following we will thus use the following construction: First we select a set of spectra that represents a typical collection of spectra for our application. From this we compute the first three eigenvectors of the corresponding correlation matrix and represent a color spectrum s with the first three coefficients in this basis. This gives us a mapping

$$s \mapsto \sigma_0(1, \xi, \eta)$$

where σ_0 is the first PCA coefficient of the spectrum. It can be shown that for all non-zero spectra s , this coefficient σ_0 is strictly positive and we can therefore use perspective projection to the plane given by coefficient value $\sigma_0 = 1$. After a suitable, global scaling it can be shown that the points with coordinates (ξ, η) in the expansion introduced above are all located on the unit disk, i. e.: $\xi^2 + \eta^2 < 1$. For these points we use complex notation $\zeta = \xi + i\eta$ and use the well-known fact that a natural set of transformations on the unit disk is defined by complex matrices M of the form:

$$M = \begin{pmatrix} \alpha & \beta \\ \bar{\beta} & \bar{\alpha} \end{pmatrix} \quad (5)$$

with $\det M = |\alpha|^2 - |\beta|^2 = 1$. These matrices act on the points on the unit disk by fractional linear transforms:

$$\zeta \mapsto M \langle \zeta \rangle = \frac{\alpha\zeta + \beta}{\bar{\beta}\zeta + \bar{\alpha}}$$

We call these transforms natural since they preserve the hyperbolic distance:

$$d_h(\zeta_1, \zeta_2) = 2 \operatorname{arctanh} \frac{|\zeta_1 - \zeta_2|}{|\zeta_1 \zeta_2 - 1|}. \quad (6)$$

and for every M we have:

$$d_h(\zeta_1, \zeta_2) = d_h(M \langle \zeta_1 \rangle, M \langle \zeta_2 \rangle) \quad (7)$$

Finally we need the following construction: We introduce the three matrices

$$J_1 = \begin{pmatrix} i & 0 \\ 0 & -i \end{pmatrix}; J_2 = \begin{pmatrix} 0 & 1 \\ 1 & 0 \end{pmatrix}; J_3 = \begin{pmatrix} 0 & i \\ -i & 0 \end{pmatrix}$$

and their linear combinations $X = \alpha_1 J_1 + \alpha_2 J_2 + \alpha_3 J_3$. For every vector $\alpha = (\alpha_1, \alpha_2, \alpha_3)$ it can be shown that e^X is of the form (5). For a given vector α and a scalar t we define

$$M(t) = e^{t(\alpha_1 J_1 + \alpha_2 J_2 + \alpha_3 J_3)}$$

It can then be shown that the points $\zeta(t)$:

$$\zeta(t) = M(t) \langle \zeta(0) \rangle = e^{tX} \langle \zeta(0) \rangle; t \in \mathbb{R} \quad (8)$$

define a curve on the unit disk. The curve starts at $\zeta(0)$ for $t=0$, its form is given by the vector α and the position of a point on the curve is given by t . A final property that is essential in the following is that every sequence $\zeta_0, \zeta_1, \zeta_2$ of points on the unit disk specifies a unique matrix M such that

$$\zeta_1 = M \langle \zeta_0 \rangle \quad \text{and} \quad \zeta_2 = M \langle \zeta_1 \rangle$$

More details about hyperbolic geometry and fractional linear transforms can be found in [12, 27] and applications of this construction to multispectral color processing are described in [13-17].

In the following we will use two constructions. In both we are given a sequence of points $\zeta_{-L}, \zeta_{-L+1}, \dots, \zeta_{-1}, \zeta_0, \zeta_1, \dots, \zeta_N$. In the first method we select the subsequence $\zeta_0, \zeta_1, \zeta_2$ and we compute the unique matrix M with $\zeta_1 = M \langle \zeta_0 \rangle, \zeta_2 = M \langle \zeta_1 \rangle = M^2 M \langle \zeta_0 \rangle$. We then estimate $\zeta_k \approx M^k \langle \zeta_0 \rangle$ for $-L \leq k \leq N$. The step length between two consecutive points is thus constant and characterized by M .

In the second method we allow arbitrary step length t_k between points ζ_k and ζ_{k+1} but we assume that all points on the sequence are located on the same curve, characterized by the parameter vector $(\alpha_1, \alpha_2, \alpha_3)$. We use an optimization process to estimate the step length parameters t_k and the vector components α_i . The optimization criterion is the accumulated hyperbolic distance between the points on the curve and the empirical measurement points ζ_k .

C. Laplacian Eigenmaps

Laplacian Eigenmaps (LE, see [1]) attempt to map data points in the high-dimensional data space to a lower dimensional space such that proximity properties between the points are preserved. This is done by considering the data points as nodes in a weighted graph and constructing the projection operator as eigenvectors of a generalized eigenvalue problem involving the *Laplace Beltrami* operator.

The following description follows the presentation of the method in [1]. The basic idea is to use the data points \mathbf{x}_i (in our case the spectral distributions) to construct a weighted graph. A "good" projection operator is an operator that maps points that are close together in the original space to points that are close together in the projection space. It can be shown that a projection operator with this property is given by the eigenvectors (with minimal eigenvalues) of a generalized eigenvalue problem.

The reduction is computed in three steps (see [1] for details):

- **Constructing the adjacency graph:** Find "neighbouring" points and put an edge between the neighbouring nodes \mathbf{x}_i and \mathbf{x}_j .
- **Compute the weight matrix:** Assign the edge linking \mathbf{x}_i and \mathbf{x}_j a weight W_{ij} describing the importance of the link between the two points connected by this edge. This defines the weight matrix \mathbf{W} .

- **Eigenmaps:** Construct the diagonal matrix D with $D_{ii} = \sum_j W_{ji}$ and $L = D - W$. L is the Laplacian matrix. The projection is defined by the solutions of the eigenvalue problem:

$$L \cdot f = \lambda \cdot D \cdot f$$

The eigenvector f_0 belonging to eigenvalue 0 is left out and the next m eigenvectors are used for embedding in the m -dimensional space.

D. Isomap

The *ISOMAP* algorithm was introduced in [25] and we follow the description there. The goal of the *ISOMAP* algorithm is to find a projection operator that best preserves the geodesic distances in the original manifold. As in the case of the *Laplacian eigenmaps* the projection operators are given by the solution of an eigenvalue problem. These solutions are constructed as follows:

ISOMAP starts with data points \mathbf{x}_i defining a graph with distances d_{ij} between neighbouring points i and j . From this the matrix D is computed where entry D_{ij} is the length of the shortest path between points i and j in the graph. Construct the squared distance matrix S with $S_{ij} = D_{ij}^2$, the "centering" matrix H with $H_{ij} = \delta_{ij} - \frac{1}{N}$ the number of data points and $\tau(D) = -\frac{HS}{2}$. For $\tau(D)$ compute the p -th eigenvector $\mathbf{v}_p = (\mathbf{v}_{1p}, \mathbf{v}_{2p}, \dots)$ with eigenvalue λ_p . Then set the p -th component of the d -dimensional coordinate vector y_i equal to $\sqrt{\lambda_p} \mathbf{v}_{1p}$. It can be shown that these eigenvectors define the projection vectors.

E. Conformal Component Analysis

Many dimensionality reduction methods are constructed with the goal to maximize proximity properties on average. This does however not insure that the geometric properties of the data space are also preserved locally. The construction of such a local geometry preserving dimensionality reduction method is described in [22]. In this approach the local geometry is measured in the form of angles and dimensionality reduction methods are required to be conformal, i. e. to preserve local angles. Such functions are known as conformal maps and the method is known as *Conformal Component Analysis*. It constructs the solution in two steps: in the first step a dimensionality reduction method like the *Laplacian Eigenmaps* is used. Then conformal eigenmaps are constructed that try to reproduce the angles in the original data space also in the new reduced space. The cost function that describes the angular distortion is based on the similarity between the angles formed by neighbouring original points and those formed by their projections. The conformal part of the algorithm constructs now a linear map of the embedding space such that the angular similarities are preserved. The solution is computed using semi-definite programming.